

Review on latest developments in random lasers with coherent feedback

Hui Cao

Department of Physics and Astronomy, Northwestern University, Evanston, IL 60208, USA

E-mail: h-cao@northwestern.edu

Received 6 September 2005, in final form 23 October 2005

Published 22 November 2005

Online at stacks.iop.org/JPhysA/38/10497

Abstract

The random laser represents a non-conventional laser whose feedback is mediated by random fluctuation of the dielectric constant in space. Depending on whether the feedback is intensity or field feedback, random lasers are classified into two categories: a random laser with incoherent and non-resonant feedback, and a random laser with coherent and resonant feedback. This paper reviews some of the latest developments in the latter, including experiments and theories on the ‘classical’ and ‘quantum’ type of random lasers with coherent feedback, the photon localization lasers. The quantum theories of random lasers are briefly introduced, followed by a discussion of the recent studies on the interplay between light localization and coherent amplification.

PACS number: 42.55.Zz

(Some figures in this article are in colour only in the electronic version)

1. Introduction

1.1. ‘LASER’ versus ‘LOSER’

A photon, unlike an electron, can stimulate an excited atom to emit a second photon into the same electromagnetic mode. This stimulated emission process is the foundation for light amplification and oscillation (i.e. self-generation). The initials of LASER refer to light amplification by stimulated emission. Nowadays, laser often means light *oscillation* by stimulated emission, which literally should be called ‘LOSER’ instead of ‘LASER’. To distinguish the above two devices, the former is called a laser amplifier, the latter a laser oscillator (Siegman 1986).

In a laser amplifier, input light is amplified when the net gain coefficient $g_{\text{eff}} = g_a - \alpha_r > 0$, where g_a and α_r represent gain and absorption coefficients, respectively. In the absence of input light, photons spontaneously emitted by excited atoms are amplified instead, giving amplified spontaneous emission (ASE).

Laser oscillation occurs when the photon generation rate exceeds the photon loss rate in a system, i.e., $g_{\text{eff}} \geq \gamma_{\text{esp}}$, where γ_{esp} is the photon escape coefficient. For example, in a Fabry-Perot cavity $\gamma_{\text{esp}} = (1/2d_m) \ln(R_1 R_2)$, where R_1 and R_2 are the reflectivities of the two mirrors and d_m is the distance between them. If gain saturation were absent, the photon number in a laser oscillator would grow to infinity in time. In other words, the rate equation for photon number would acquire an unstable solution above the oscillation threshold. In reality, gain saturation reduces g_{eff} to γ_{esp} so that the photon generation rate is balanced by the photon loss rate and the number of photons in the oscillator reaches a finite steady-state value.

1.2. Random laser

For a long time, optical scattering was considered detrimental to laser because such scattering removes photons from the lasing modes of a conventional laser cavity. However, in a disordered medium with gain, light scattering plays a positive role in both laser amplification and laser oscillation. Multiple scattering increases the path length or dwell time of light in an active medium, thus enhancing laser amplification. In addition, recurrent light scattering could provide coherent feedback for laser oscillation.

Since the pioneering work of Letokhov and co-workers (Ambartsumyan *et al* 1970), lasing in disordered media has been the subject of intense theoretical and experimental studies. It represents the process of light amplification by stimulated emission with feedback mediated by random fluctuation of the dielectric constant in space. There are two kinds of feedback: one is *intensity* or *energy* feedback, the other is *field* or *amplitude* feedback (Cao *et al* 2001). The field feedback is phase sensitive (i.e. coherent), and therefore frequency dependent (i.e. resonant). The intensity feedback is phase insensitive (i.e. incoherent) and frequency independent (i.e. non-resonant). Based on the feedback mechanisms, random lasers are classified into two categories: (i) random laser with incoherent and non-resonant feedback; (ii) random laser with coherent and resonant feedback (Cao *et al* 2000a, 2003b). This paper summarizes the latest developments in (ii). A brief review on (i) can be found in, e.g., Cao (2003).

Random lasers have been realized mostly in disordered dielectric media of finite size. They differ from the chaotic cavity lasers which have been a focus of many theoretical studies (Beenakker 1999, Tureci *et al* 2005). In the latter, the cavity is nearly closed with metallic boundary. Its dimension is much larger than the wavelength λ of radiation. There are a few openings at the boundary but their size is smaller than λ . Owing to the irregular shape of the boundary and/or scatterers placed at random positions inside the cavity, the intra-cavity ray dynamics is chaotic. The small leakage rate allows light to ergodically explore the entire cavity volume. In contrast, the random lasers considered in this paper have completely open boundaries, and light can escape from the dielectric random media via any point on the boundaries. Hence, they are open systems with strong coupling to the environment.

1.3. Characteristic length scales for a random laser

1.3.1. Correlation radius R_c . In a disordered dielectric medium, the dielectric constant $\epsilon(\mathbf{r})$ fluctuates randomly in space. The spatial variation of $\epsilon(\mathbf{r})$ can be characterized statistically by the correlator $K(\Delta\mathbf{r}) \equiv \langle \epsilon(\mathbf{r})\epsilon(\mathbf{r} + \Delta\mathbf{r}) \rangle$, where $\langle \dots \rangle$ represents ensemble average. When the random medium is isotropic, the width of $K(\Delta r)$ is called the correlation radius R_c . It reflects the length scale of spatial fluctuation of dielectric constant. If $R_c \gg \lambda$, light is deflected by long-range disorder. When R_c is comparable to or less than λ , light is scattered by short-range disorder.

1.3.2. Scattering mean free path l_s and transport mean free path l_t . The relevant length scales that describe light scattering process are the scattering mean free path l_s and the transport mean free path l_t . The scattering mean free path l_s is defined as the average distance that light travels between two consecutive scattering events. The transport mean free path l_t is defined as the average distance a wave travels before its direction of propagation is randomized. These two length scales are related by

$$l_t = \frac{l_s}{1 - \langle \cos \theta \rangle}. \quad (1)$$

where $\langle \cos \theta \rangle$ is the average cosine of the scattering angle, which can be found from the differential scattering cross section. Rayleigh scattering is an example of $\langle \cos \theta \rangle = 0$ or $l_t = l_s$, while Mie scattering may have $\langle \cos \theta \rangle \approx 0.5$ or $l_t \approx 2l_s$.

1.3.3. Gain length l_g and amplification length l_{amp} . Light amplification by stimulated emission in a random medium is described by the gain length l_g and the amplification length l_{amp} . The gain length l_g is defined as the path length over which light intensity is amplified by a factor e . The amplification length l_{amp} is defined as the (rms) average distance between the beginning and ending points for paths of length l_g . In a homogeneous medium, light travels in a straight line, thus $l_{\text{amp}} = l_g$. In the diffusive sample, $l_{\text{amp}} = \sqrt{D\tau_{\text{amp}}}$, where D is the diffusion coefficient, $\tau_{\text{amp}} = l_g/v$, v is the speed of light. In a three-dimensional (3D) system, $D = vl_t/3$, thus

$$l_{\text{amp}} = \sqrt{\frac{l_t l_g}{3}}. \quad (2)$$

The gain length l_g is the analogue of the inelastic length l_i defined as the travel length over which light intensity is reduced to $1/e$ by absorption. Hence, the amplification length l_{amp} is analogous to the absorption length $l_{\text{abs}} = \sqrt{l_t l_i/3}$.

1.3.4. Dimensionality d and size L . Light transport in a random medium depends on its dimensionality d and size L . For a random medium of $d > 1$, L refers to its smallest dimension. The average trapping time of photons in a diffusive random medium is $\tau_d = L^2/D$. In an active random medium, the gain volume may be smaller than the volume of the entire random medium, e.g., when only part of the disordered medium is pumped. The gain volume is characterized by its dimension L_g , and $L_g \leq L$.

1.4. Light localization

There are three regimes for light transport in a 3D random medium: (i) ballistic regime, $L \sim l_t$; (ii) diffusive regime, $L \gg l_t \gg \lambda$; (iii) localization regime, $kl_t \simeq 1$ (k is the wave vector in the random medium) (John 1991).

Light localization can also be understood in the mode picture. Quasimodes, also called quasi-states, are the eigenmodes of the Maxwell equations in a passive random medium. Due to the finite size of a dielectric medium and its open boundary, the frequency of a quasimode is a complex number: $\Omega = \omega_r + i\gamma$. γ is the decay rate of a quasimode as a result of its coupling to the environment. It also represents the linewidth of the quasimode in frequency. The Thouless number δ is defined as the ratio of average linewidth $\delta\nu = \langle \gamma \rangle$ to average frequency spacing $d\nu$ of quasimodes, $\delta \equiv \delta\nu/d\nu$. In the delocalization regime, quasimodes overlap in frequency, $\delta > 1$. In the localization regime, quasimodes do not overlap, $\delta < 1$. The localization threshold is set at $\delta = 1$, that is the Thouless criterion. Thus, the localization transition corresponds to a transition from overlapping modes to non-overlapping modes.

The openness of a random laser, namely, its coupling to the environment, can be characterized by δ . Note that the value of δ is obtained in the absence of gain or absorption so that it describes solely light leakage from the random system. Typical chaotic cavity lasers and photon localization lasers have non-overlapping modes, $\delta < 1$, whereas in the diffusive random lasers most quasimodes overlap, $\delta > 1$.

1.5. 'Classical' versus 'quantum' random lasers

Random lasers with coherent feedback can operate either in the classical optics regime or in the wave optics regime (Polson *et al* 2002). In the former $R_c \gg \lambda$, whereas in the latter $R_c \sim \lambda$. They have analogues in chaotic cavity lasers whose cavity shape is irregular. In the classical regime, the spatial variation of chaotic cavity shape is much larger than the wavelength of radiation, whereas in the quantum/wave regime the spatial variation is comparable to or smaller than the wavelength.

In a random medium, when the dielectric constant varies over length scale much larger than λ , geometrical optics can be applied to describe light propagation in terms of ray trajectories. The majority of the ray trajectories are chaotic and open, yet unstable periodic orbits exist when the sample size is large enough. In an open system, unstable periodic orbits might trap light for a longer time than chaotic trajectories. Thus, lower optical gain is needed to realize lasing oscillation in certain 'scar' modes that concentrate on some unstable periodic orbits.

When the dielectric constant fluctuates over length scales comparable to or even smaller than λ , ray optics no longer holds. It is replaced by wave optics that not only describes light scattering by short-range disorder but also takes into account interference of scattered waves. The interference effect is crucial to light localization in a random medium, which is analogous to the (quantum) Anderson localization of electron in a short-range potential. Even when $l_t > \lambda$, light may still be trapped partially in a random medium via the process of multiple scattering and wave interference. The incomplete confinement can be compensated by photon amplification when optical gain is introduced to a random medium, leading to lasing oscillation.

2. Classical random laser with coherent feedback

The classical type of random lasers with coherent feedback were first demonstrated by Vardeny and co-workers in weakly disordered media such as π -conjugated polymer films (Frolov *et al* 1999a, Polson *et al* 2001b), organic dye-doped gel films (Frolov *et al* 1999b), synthetic opals infiltrated with π -conjugated polymers and dyes (Frolov *et al* 1999b, Yoshino *et al* 1999, Polson *et al* 2001a). The long-range fluctuations of refractive index in their polymer films are most likely caused by inhomogeneity of the film thickness. Since light is confined within a film due to waveguiding, larger thickness leads to higher effective index of refraction.

2.1. Lasing phenomenon

Experimentally, the samples are excited by short laser pulses. The broad photoluminescence band at low pumping narrows drastically with increasing pump intensity. As the excitation intensity increases even further, the emission spectrum transforms into a fine structure that consists of a number of sharp peaks. The spectral width of these peaks is less than 1 nm. When the pump light excites a different sample or a different part of the same sample, the narrow peaks change completely. However, when the same part of the sample is excited repeatedly by different pump pulses, the spectral peaks are reproducible.

Polson *et al* (2002) suggest that the lasing modes in the polymer films are formed by total internal reflection at the boundaries of high refractive index regions. The long-range fluctuation of the refractive index is similar to a ring resonator, in the sense that it gives rise to a number of localized modes having close frequencies and quality factors. These modes are revealed in the emission spectrum. Since the frequencies of such modes are correlated, they can estimate the size, L_r , of the underlying resonators from the power Fourier transform (PFT) of lasing spectra. They indeed find $L_r \gg \lambda$ in their samples.

Along with the long-range fluctuation of refractive index, short-range disorder is also present in the polymer films. The ability of most random resonators to trap light by total internal reflection is suppressed by the short-range disorder. The dramatic consequence of this suppression is that the resonators that ‘survive’ the short-range disorder are sparse, and consequently almost identical. Experimentally, despite the PFT of individual random lasing spectra exhibiting position-specific multi-peak structures, averaging the PFTs over the sample positions does not smear these features, but in contrast yields a series of distinct transform peaks. Moreover, the shape of the averaged PFT is universal, i.e., increasing the disorder and correspondingly reducing l_t do not change this shape: the average of the PFT spectra at different l_t scales with l_t to a universal curve (Polson *et al* 2002).

2.2. Almost localized states

To understand the classical type of random laser with coherent feedback, Apalkov, Raikh and Shapiro have made a comprehensive theoretical analysis (Apalkov *et al* 2003). They believe that the lasing modes are the almost localized states in the passive medium. Such states are formed due to some rare disorder configurations that can trap light for a long time in a sub-mean-free-path region in space. The almost localized states are non-universal, i.e., their character and formation probability depend on not only the average strength of disorder, but also the microscopic details of disorder (Apalkov *et al* 2004a).

In the case of a continuous random potential, the almost localized states are confined to small rings of a sub mean-free-path size. Apalkov, Raikh and Shapiro calculate the areal density of the almost localized states in a film with fluctuating refractive index (Apalkov *et al* 2002). The rings formed by disorder can be viewed as waveguides that support the whispering-gallery type modes. Because of the azimuthal symmetry, these modes are characterized by the angular momentum, m . The areal density of ring resonators with quality factor Q can be expressed as $N_m(kl_t, Q) = N_0 \exp[-S_m(kl_t, Q)]$ for $kl_t > 1$. In the case of smooth disorder $kR_c \gg 1$, $S_m \sim l_t (\ln Q)^{4/3} / (kR_c^2 m^{1/3})$. In the opposite limit of short-range disorder, $S_m \sim kl_t \ln Q$. Therefore, when on average the light propagation is diffusive, the likelihood for finding an almost localized state increases sharply with the disorder correlation radius R_c for a given kl_t . Note that this conclusion applies only to a continuous (Gaussian) random potential. In the presence of discrete lattice (the Anderson model), a new type of almost localized state is formed, whose formation probability is reduced by correlation in disorder (Patra 2003b, Apalkov *et al* 2004b).

Apalkov and Raikh also investigate the fluctuation of the random lasing threshold (Apalkov and Raikh 2005). They find that the distribution of the threshold gain over the ensemble of statistically independent finite-size samples is universal. This universality stems from two results: (i) the lasing threshold in a given sample is determined by the highest quality mode of all the random resonators present in the sample; (ii) the areal density of the random resonators decays sharply with the quality factor of the mode that they trap. In a 2D sample of area S , the distribution function of the threshold excitation intensity I_{th} is

$$F_S(I_{\text{th}}) = \frac{\beta_S}{I_{\text{th}}} \left(\frac{I_{\text{th}}}{I_S} \right)^{-\beta_S} \exp \left[\left(\frac{I_{\text{th}}}{I_S} \right)^{-\beta_S} \right]. \quad (3)$$

The typical value I_S is related to the sample area S :

$$I_S \propto \exp \left\{ - \left[\frac{\ln(S/S_0)}{G} \right]^{1/\alpha} \right\}. \quad (4)$$

S_0 is the typical area of a random resonator. The parameters α and G are determined by the intrinsic properties of the disordered medium and are independent of S . These two parameters play different roles: α is determined exclusively by the shape of the disorder correlator and G is a measure of the disorder strength. $\beta_S \propto [\ln(S/S_0)]^{(\alpha-1)/\alpha}$. Parameter β_S decreases with kl_t as a power law, and the exponent depends on the microscopic properties of the disorder. For a weakly scattering medium, $\beta_S \gg 1$, and $F_S(I_{\text{th}})$ is close to a Gaussian distribution, $F_S(I_{\text{th}}) \propto \exp[-(\beta_S^2/2)(I_{\text{th}}/I_S - 1)^2]$. When β_S is small, the distribution $F_S(I_{\text{th}})$ is broad and strongly asymmetric. It has a long tail towards the high thresholds and falls off abruptly towards low thresholds.

3. Quantum random laser with coherent feedback

In the classical type of random lasers with coherent feedback, formation of (closed) periodic orbits with small leakage results in light confinement. The interference effect plays a secondary role as it only determines the resonant frequencies in the periodic orbits. However, in the quantum type of random lasers with coherent feedback, the random media have discrete scatterers and strong short-range disorder, thus the interference of scattered waves is essential to light trapping in a random medium. The active random media used for the quantum type of random lasers can be divided into two categories: (i) aggregation of active scatterers; (ii) passive scatterers in continuous gain media. Both have their advantages and disadvantages. In (ii), gain media and scattering centres are separated, which allows independent variation of the amounts of scattering and gain. However, the scattering strength in (i) is usually higher than that in (ii), owing to larger contrast of refractive index and higher density of scatterers. In the following subsections, lasing in both types of random media is discussed with some examples.

3.1. Lasing oscillation in semiconductor nanostructures

Figure 1 shows the scanning electron microscope (SEM) images of some semiconductor nanostructures that are used in our random laser experiments. The ZnO nanorods in figure 1(a) are grown on a sapphire substrate by metalorganic chemical vapour deposition (MOCVD). The rods are uniform in diameter and height, but randomly located on the substrate. The average rod diameter is about 50 nm. The ZnO nanorod array is a two-dimensional (2D) scattering system, as light is scattered by the nanorods in the plane perpendicular to the rods. When the layer of ZnO nanorods has larger refractive index than the substrate, index guiding leads to light confinement in the third direction parallel to the rods. Figure 1(b) shows the ZnO nanoparticles synthesized in a wet chemical reaction. The particles are polydisperse with an average size ~ 100 nm. They are closely but randomly packed with a filling fraction $\sim 50\%$. Since light is scattered by ZnO nanoparticles in all directions, the ZnO powder represents a 3D scattering system. The above two examples of random media have discrete scatterers of subwavelength size. The short-range disorder results in strong light scattering. In the ZnO powder, the transport mean free path $l_t \sim \lambda$.

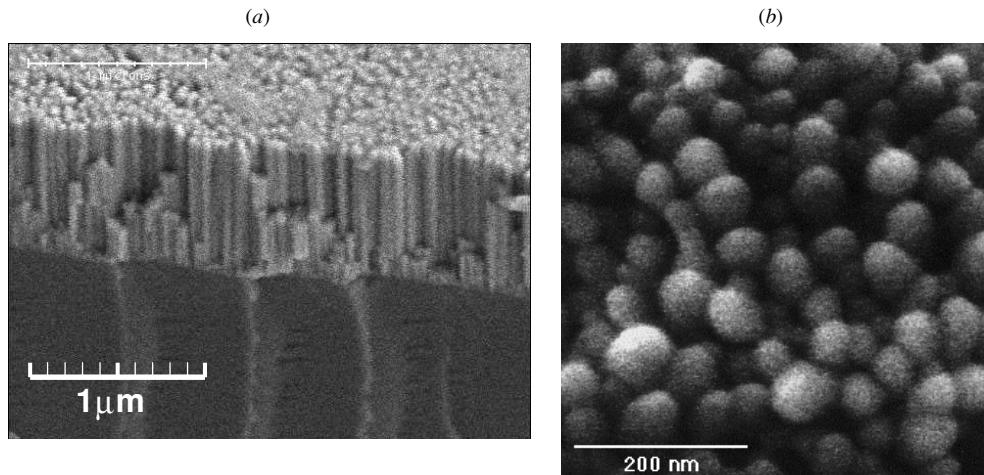


Figure 1. SEM images of (a) ZnO nanorods on a sapphire substrate and (b) closely packed ZnO nanoparticles.

To introduce optical gain, the ZnO samples are optically pumped by the frequency-tripled output ($\lambda = 355$ nm) of a mode-locked Nd:YAG laser (10 Hz repetition rate, 20 ps pulse width). The ZnO nanorods and nanoparticles become active scatterers. We simultaneously record the emission spectrum and image the spatial distribution of emitted light intensity on the sample surface.

We observe lasing with coherent resonant feedback in both ZnO nanorods and nanoparticles. Since their lasing phenomena are similar, the measurement results of ZnO powder are presented next. Figure 2 shows the measured spectra and spatial distribution of emission in a ZnO powder film at two pumping intensities. At low pumping level, the spectrum consists of a single broad spontaneous emission band. Its full width at half maximum (FWHM) is about 12 nm (figure 2(a)). In figure 2(b), the spatial distribution of the spontaneous emission intensity is smooth across the excitation area. Due to the pump intensity variation over the excitation spot, the spontaneous emission in the centre of the excitation spot is stronger. When the pump intensity exceeds a threshold, discrete narrow peaks emerge in the emission spectrum (figure 2(c)). The FWHM of these peaks is about 0.2 nm. Simultaneously, bright tiny spots appear in the image of the emitted light distribution in the film (figure 2(d)). The size of the bright spots is between 0.3 and 0.7 μm . When the pump intensity is increased further, additional sharp peaks emerge in the emission spectrum, and more bright spots appear in the image of the emitted light distribution. Above the threshold, the total emission intensity increases much more rapidly with the excitation intensity.

The frequencies of the sharp peaks depend on the sample position. As we move the excitation spot across the sample, the frequencies of these peaks change completely. However, at a fixed sample position, the peak frequencies remain the same, while the peak heights vary from shot to shot due to fluctuation of pump pulses. These phenomena suggest that the discrete spectral peaks result from spatial resonances for light in the ZnO powder, and such resonances are related to the local configurations of ZnO particles. Due to local variation in particle density and spatial configuration, there exist small regions of stronger scattering. Light can be trapped in these regions through the process of recurrent scattering and interference. For a particular configuration of ZnO nanoparticles, only light at certain frequencies can be confined, because the interference effect is frequency sensitive. In a different part of the sample, the

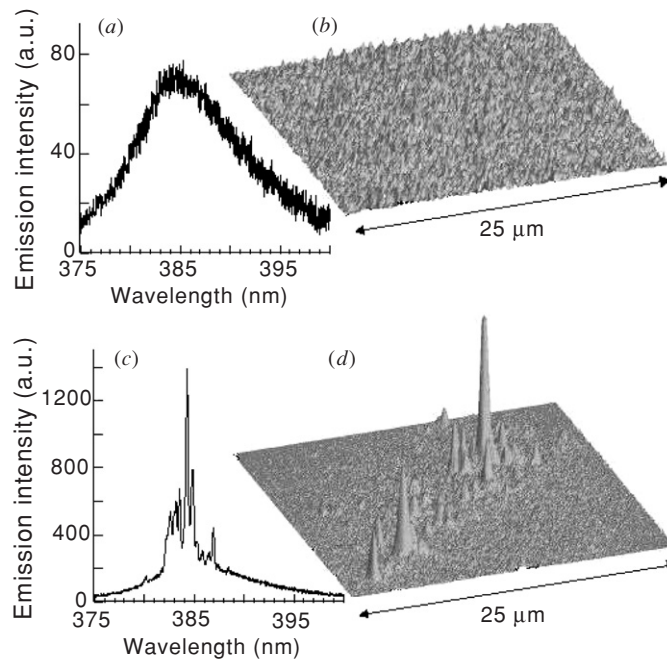


Figure 2. (a) and (c) are the measured spectra of emission from the ZnO powder. (b) and (d) are the measured spatial distribution of emission intensity on the sample surface. The incident pump pulse energy is 5.2 nJ for (a) and (b), and 12.5 nJ for (c) and (d).

particle configuration is different, thus light at different frequencies is confined. However, the confinement is incomplete as light can escape through the sample surface. When the photon generation rate reaches the photon escape rate, lasing oscillation occurs at the local resonant frequencies, that gives discrete lasing peaks in the emission spectrum.

We investigate the dependence of random laser on the pump area A_p . The lasing threshold decreases with increasing A_p , as it is more likely to find a stronger trapping site for light within a larger gain volume. At a fixed pump intensity, more lasing peaks appear when A_p increases. It is simply because there are more trapping sites for light. Eventually at very large pump area, the lasing peaks are so close to each other in frequency that they can no longer be resolved. Instead, they merge into a broad band. However, when A_p is reduced to below a critical value, lasing oscillation stops. The critical pump area decreases with increasing pumping level. The higher the pumping level, the less confinement of light is required to reach the lasing threshold, the more likely to find such an incomplete trapping site in a smaller region.

The temporal evolution of emission is measured by a streak camera (Soukoulis *et al* 2002). Below the lasing threshold, the decay time of the emission is 167 ps. When the pump intensity exceeds the threshold, the emission pulse is shortened dramatically. The initial decay of emission intensity is very fast; the decay time is 27 ps. After about 50 ps, the fast decay is replaced by a slow decay. The later decay time is 167 ps, which is equal to the decay time below the threshold. We believe that the initial fast decay is caused by rapid stimulated emission, and the later slow decay results from spontaneous emission and nonradiative recombination. As the pump intensity increases further, the initial stimulated emission becomes much stronger than the later spontaneous emission. We also investigate the dynamics of individual lasing

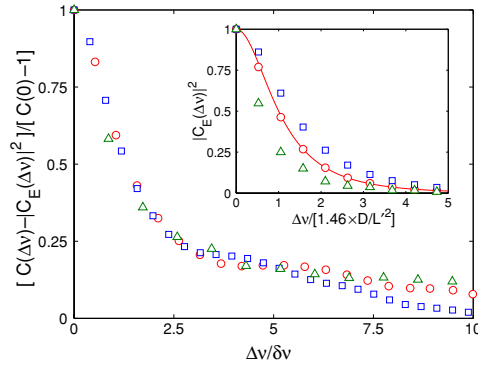


Figure 3. Spectrally integrated intensity of emission from the ZnO microcluster as a function of the incident pump pulse energy. The inset is the SEM image of the microcluster.

modes by combining a spectrometer with a streak camera. The time traces of individual lasing modes reveal that lasing in different modes is not synchronized. Just above the lasing threshold, relaxation oscillation is observed for some of the lasing modes. Since the pump pulse is shorter than both radiative and nonradiative recombination times of ZnO particles, lasing is in the transient regime. Recently, lasing in ZnO powder has been realized with 10 ns pump pulses (Markushev *et al* 2005). Since the pumping time is much longer than all the characteristic time scales in the ZnO powder, the lasing oscillation could be regarded as quasi-continuous.

The quantum statistical property of laser emission from the ZnO powder is also probed in a photon counting experiment (Cao *et al* 2001). For a single-mode coherent light, the photon number distribution satisfies the Poisson distribution, whereas for a single-mode chaotic light the photon number distribution meets the Bose–Einstein distribution. However, for a multimode chaotic light, the photon number distribution approaches the Poisson distribution as the number of modes increases to infinity. Hence, it would be difficult to distinguish coherent light from chaotic light in the multimode measurement. Experimentally, we count photons in a single electromagnetic mode, i.e. the counting time is shorter than the inverse of frequency bandwidth of a lasing mode, and the collection angle in the far-field zone is less than one angular speckle. We find that the photon number distribution in a single mode changes continuously from the Bose–Einstein distribution near the threshold to the Poisson distribution well above the threshold. The second-order correlation coefficient G_2 decreases gradually from 2 to 1. It is well known that for a single-mode chaotic light $G_2 = 2$, while for a single-mode coherent light $G_2 = 1$. Hence, coherent light is indeed generated in the highly disordered ZnO powder.

3.2. Micro random laser

Employing a spectrally resolved speckle technique (Cao *et al* 2002), we find that the lasing modes in closely packed ZnO nanoparticles can be as small as a couple of microns. This means strong optical scattering not only supplies coherent feedback for lasing, but also leads to spatial confinement of laser light in micron-size volume (Cao *et al* 2000b). This allows us to realize a new type of microlasers that are made of disordered media (Cao *et al* 2000c).

The inset of figure 3 is a SEM image of a microcluster of ZnO nanoparticles. The size of the cluster is about 1.7 μm . It contains roughly 20 000 ZnO nanoparticles. A

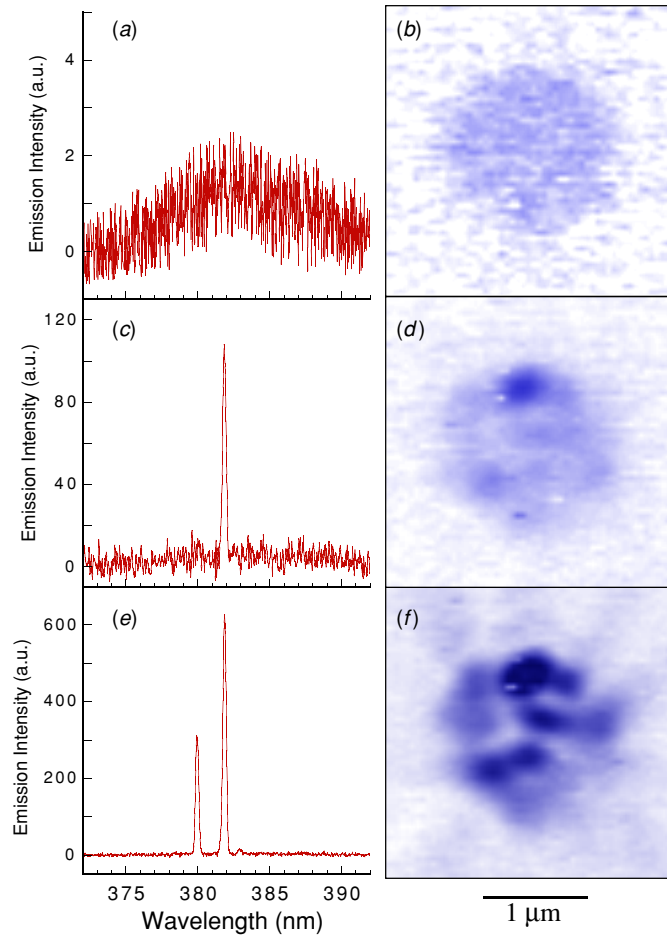


Figure 4. (a), (c) and (e) are the spectra of emission from the ZnO microcluster shown in figure 3. (b), (d) and (f) are the corresponding spatial distribution of emission intensity in the microcluster. The incident pump pulse energy is 0.26 nJ for (a) and (b), 0.35 nJ for (c) and (d), and 0.50 nJ for (e) and (f).

single cluster is optically pumped by the third harmonics of a pulsed Nd:YAG laser. At low pumping level, the emission spectrum consists of a single broad spontaneous emission peak (figure 4(a)). Its FWHM is 12 nm. The spatial distribution of the spontaneous emission intensity is uniform across the cluster (figure 4(b)). When the pump intensity exceeds a threshold, a sharp peak emerges in the emission spectrum (figure 4(c)). Its FWHM is 0.2 nm. Simultaneously, a couple of bright spots appear in the image of the emitted light distribution in the cluster (figure 4(d)). When the pump intensity increases further, a second sharp peak emerge in the emission spectrum (figure 4(e)). Correspondingly, additional bright spots appear in the image of the emitted light distribution (figure 4(f)). Note that the frequencies of the sharp peaks and the positions of the bright spots do not change from pump pulse to pulse (shot).

The total emission intensity is plotted against the pump intensity in figure 3. The curve exhibits a distinct slope change at the threshold where sharp spectral peaks and bright spots

appear. Well above the threshold, the total emission intensity increases almost linearly with the pump intensity. These data reveal lasing oscillation in the micron-size cluster.

Since the cluster is very small, optical reflection from the boundary of the cluster may have some contribution to light confinement in the cluster (Wiersma 2000, Kretschmann and Maradudin 2004). However, the laser cavity is not formed by total internal reflection at the boundary. Otherwise, the spatial pattern of laser light would be a bright ring near the edge of the cluster (Taniguchi *et al* 1996). We believe that the 3D optical confinement in a micron-size ZnO cluster is realized through multiple scattering and interference. Since interference effect is wavelength sensitive, only light at certain wavelengths can be confined in a cluster. In another cluster of different particle configuration, light at different wavelengths is confined. Therefore, the lasing frequencies are fingerprints of individual random clusters.

3.3. Collective modes of resonant scatterers

A simplified way of simulating the closely packed ZnO nanoparticles or nanorods is to approximate individual particles or rods as dipolar oscillators (Burin *et al* 2001). We calculate the quasimodes in a random ensemble of point dipoles. The k th dipolar oscillator is represented by its resonant frequency ω_k and transition dipole moments \mathbf{d}_k , where $k = 1, 2, \dots, N$. N is the total number of scatterers. The gain is introduced into each scatterer by adding an imaginary term $i\tilde{g}$ to its resonant frequency. A quasimode of this system represents a collective excitation of the coupled dipoles, thus it is also called a collective mode. The equation of motion for the k th oscillator's polarization component $\mathbf{p}_k = p_k \mathbf{d}_k / d_k$ can be written as

$$-\Omega^2 p_k = -(\omega_k - i\tilde{g})^2 p_k + 2\omega_k d_k (\mathbf{d}_k \cdot \mathbf{E}_k). \quad (5)$$

\mathbf{E}_k is the local electric field,

$$\mathbf{E}_k = \sum_{j \neq k} \mathbf{E}_{kj} + i\frac{2}{3}q^3 \mathbf{p}_k, \quad (6)$$

where $q = \Omega/c$ and \mathbf{E}_{kj} represents the electric field generated by the j th dipole at the location of k th dipole. The solution to the Maxwell equations for electric field of a single dipole gives

$$\mathbf{E}_{kj} = e^{iqR_{kj}} \frac{\mathbf{p}_j - 3\mathbf{n}_{kj}(\mathbf{n}_{kj} \cdot \mathbf{p}_j)}{R_{kj}^3} (1 - iqR_{kj}) + q^2 e^{iqR_{kj}} \frac{\mathbf{p}_j - \mathbf{n}_{kj}(\mathbf{n}_{kj} \cdot \mathbf{p}_j)}{R_{kj}}, \quad (7)$$

where $\mathbf{n}_{kj} = \mathbf{R}_{kj}/R_{kj}$, \mathbf{R}_{kj} is the vector from the j th dipole to the k th dipole.

There are N solutions to the above equations for N coupled dipolar oscillators. Hence, there are N collective modes, each characterized by a complex frequency Ω_α ($\alpha = 1, 2, \dots, N$). The imaginary part of Ω_α , γ_α , represents the decay rate of a collective mode caused by light leakage out of the system. In the absence of gain $\tilde{g} = 0$, all decay rates are positive and the system is lossy. An increase of gain leads to a decrease of γ_α . At some finite value of gain g_{th} , the decay rate for some collective mode vanishes. It corresponds to the onset of lasing instability. The collective mode with the smallest decay rate in the passive system ($\tilde{g} = 0$) turns out to be the first lasing mode.

We numerically calculate the threshold gain \tilde{g}_{th} in 2D random arrays of dipolar oscillators with N up to 1000. First, we assume that all the dipoles have the same resonant frequency: $\omega_k = \omega_0$. They are positioned randomly within a circle of radius R_0 . The average inter-dipole distance, normalized by the resonant wavelength $\lambda_0 = 2\pi c/\omega_0$, is described by $\eta = 2\pi R_0/\sqrt{N}$. The ensemble-averaged lasing threshold decreases with increasing N as $\langle g_{\text{th}} \rangle \propto N^{-\beta}$, where the exponent β is a function of η . It is equivalent to $1/A^\beta$ dependence on the sample area A for a fixed particle density. Our numerical simulation gives $\beta = 0.52$ for $\eta = 0.3$, $\beta = 0.51$ for $\eta = 1$ and $\beta = 0.335$ for $\eta = 3$. The spatial size of the

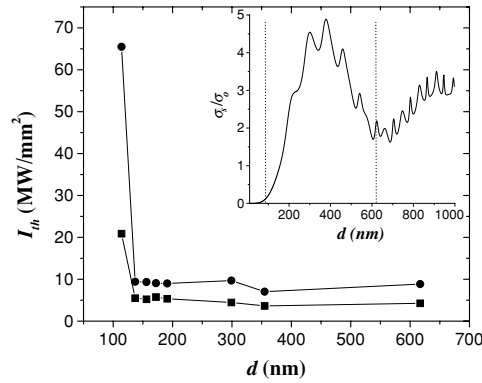


Figure 5. The incident pump intensity at lasing threshold I_{th} versus ZnO sphere diameter d_s . Squares and circles correspond to the pump spot diameter of $8 \mu\text{m}$ and $16 \mu\text{m}$, respectively. Inset shows the normalized scattering cross section σ_{sc}/σ_g of single ZnO sphere as a function of its diameter d_s .

lasing modes is usually smaller than that of the entire system. Hence, the decrease of \tilde{g}_{th} with the system size results from the increase in the probability of finding optimum particle configurations for minimum γ_α rather than the formation of larger modes. Next, we gradually introduce dispersion into the resonant frequencies ω_k of dipolar oscillators. As the dispersion increases, the efficiency of forming collective modes with small γ_α decreases. The threshold gain \tilde{g}_{th} becomes nearly size independent when ω_k deviates from each other by more than the near-neighbour dipolar coupling constant.

Therefore, the collective excitations can be formed most efficiently when the scatterers are in resonance with each other (Burin *et al* 2001). This condition can be realized experimentally with ZnO particles of uniform shape and size (Wu *et al* 2004b). We have developed a two-stage chemical reaction process to synthesize monodisperse ZnO spheres (Seelig *et al* 2003). The mean diameter of ZnO spheres is varied from 85 nm to 617 nm. The dispersion of the sphere diameter is 5–8%. High-resolution SEM images reveal that individual spheres consist of numerous ZnO nanocrystallites of size less than 10 nm. The porosity of ZnO spheres reduces the refractive index to ~ 1.7 . The ZnO spheres are closely packed with the volume fraction $\sim 58\%$. Figure 5 is a plot of the lasing threshold pump intensity I_{th} versus the mean diameter d_s of ZnO spheres for two pump areas. I_{th} decreases drastically with increasing sphere diameter from 85 nm to 137 nm. This rapid drop is replaced by a slow decrease as d_s increases from 137 nm to 355 nm. When d_s increases further to 617 nm, I_{th} increases slightly. The variation of I_{th} with d_s follows roughly the trend of scattering cross section σ_{sc} of ZnO spheres. The inset of figure 5 shows the ratio of σ_{sc} to σ_g (geometrical cross section) of a single ZnO sphere as a function of its diameter d_s at the lasing wavelength 375 nm. The dotted lines mark the range of the diameters of ZnO spheres we fabricate. The range of d_s in our random lasing experiment covers the first few Mie resonances at the ZnO emission wavelength. σ_{sc} exhibits a drastic increase with d_s before reaching the first Mie resonance at $d_s \sim 200$ nm. The Mie resonances are broad owing to relatively low refractive index of ZnO spheres. The value of σ_{sc} reaches the maximum at $d_s \sim 370$ nm. Then, it starts decreasing with a further increase of d_s to 617 nm. At the Mie resonances, photon dwell time within individual scatterers which have optical gain is drastically increased, leading to a significant enhancement of light amplification. Of course in such densely packed system as ours, scattering particles cannot be considered independent; the resonances of individual scatterers are significantly modified by the interactions among

them. Strong coupling of resonant scatterers lead to formation of collective modes with small as well as large decay rates (Ripoll *et al* 2004, Vanneste and Sebbah 2005). The former serve as the lasing modes. The experimental data of I_{th} can be explained qualitatively in terms of σ_{sc} . The larger the scattering cross section of individual spheres, the stronger the coupling among them, the higher the chance of forming collective modes with smaller decay rates. Thus, the lasing threshold is lower.

3.4. Time-dependent theory of random laser

Simulation of random lasers above the threshold requires a time-dependent model that takes into account the gain saturation effect. Jiang and Soukoulis have developed a time-dependent theory for random laser that couples the Maxwell equations with the rate equations of electronic population (Jiang and Soukoulis 2000). The gain medium is the four-level electronic material. Electrons are pumped from level 0 to level 3, then relax quickly (with time constant τ_{32}) to level 2. Level 2 and level 1 are the upper and lower levels of the lasing transition at frequency ω_a . After radiative decay (with time constant τ_{21}) from level 2 to 1, electrons relax rapidly (with time constant τ_{10}) from level 1 back to level 0. The populations in four levels (N_3, N_2, N_1, N_0) satisfy the following rate equations:

$$\begin{aligned}\frac{dN_3(\mathbf{r}, t)}{dt} &= P_r(t)N_0(\mathbf{r}, t) - \frac{N_3(\mathbf{r}, t)}{\tau_{32}}, \\ \frac{dN_2(\mathbf{r}, t)}{dt} &= \frac{N_3(\mathbf{r}, t)}{\tau_{32}} + \frac{\mathbf{E}(\mathbf{r}, t)}{\hbar\omega_a} \cdot \frac{d\mathbf{P}(\mathbf{r}, t)}{dt} - \frac{N_2(\mathbf{r}, t)}{\tau_{21}}, \\ \frac{dN_1(\mathbf{r}, t)}{dt} &= \frac{N_2(\mathbf{r}, t)}{\tau_{21}} - \frac{\mathbf{E}(\mathbf{r}, t)}{\hbar\omega_a} \cdot \frac{d\mathbf{P}(\mathbf{r}, t)}{dt} - \frac{N_1(\mathbf{r}, t)}{\tau_{10}}, \\ \frac{dN_0(\mathbf{r}, t)}{dt} &= \frac{N_1(\mathbf{r}, t)}{\tau_{10}} - P_r(t)N_0(\mathbf{r}, t).\end{aligned}\tag{8}$$

$P_r(t)$ represents the external pumping rate. $\mathbf{P}(\mathbf{r}, t)$ is the polarization density that obeys the equation

$$\frac{d^2\mathbf{P}(\mathbf{r}, t)}{dt^2} + \Delta\omega_a \frac{d\mathbf{P}(\mathbf{r}, t)}{dt} + \omega_a^2\mathbf{P}(\mathbf{r}, t) = \frac{\Gamma_r}{\Gamma_c} \frac{e^2}{m} [N_1(\mathbf{r}, t) - N_2(\mathbf{r}, t)]\mathbf{E}(\mathbf{r}, t).\tag{9}$$

ω_a and $\Delta\omega_a$ represent the centre frequency and linewidth of the atomic transition from level 2 to level 1, respectively. $\Gamma_r = 1/\tau_{21}$, $\Gamma_c = e^2\omega_a^2/6\pi\epsilon_0 mc^3$, where e and m are electron charge and mass, respectively. $\mathbf{P}(\mathbf{r}, t)$ introduces gain to the Maxwell equations:

$$\nabla \times \mathbf{E}(\mathbf{r}, t) = -\frac{\partial \mathbf{B}(\mathbf{r}, t)}{\partial t},\tag{10}$$

$$\nabla \times \mathbf{H}(\mathbf{r}, t) = \epsilon(\mathbf{r})\frac{\partial \mathbf{E}(\mathbf{r}, t)}{\partial t} + \frac{\partial \mathbf{P}(\mathbf{r}, t)}{\partial t},\tag{11}$$

where $\mathbf{B}(\mathbf{r}, t) = \mu\mathbf{H}(\mathbf{r}, t)$. The disorder is described by the spatial fluctuation of the dielectric constant $\epsilon(\mathbf{r})$. The Maxwell equations are solved with the finite-difference time-domain (FDTD) method (Taflove and Hagness 2000) to obtain the electromagnetic field distribution in the random medium. Fourier transform of $\mathbf{E}(\mathbf{r}, t)$ gives the local emission spectrum. To simulate an open system, the random medium has a finite size and it is surrounded by air. The surrounding air is terminated by strongly absorbing layers, e.g. the uniaxial perfectly matched layers that absorb all the light escaping through the boundary of the random medium. Within a semiclassical framework, the spontaneous emission can be included in the Maxwell equations as a noise current.

Jiang and Soukoulis simulate the lasing phenomenon in a 1D random system with the time-dependent theory. A critical pumping rate exists for the appearance of lasing peaks in the spectrum. The number of lasing modes increases with the pumping rate and the length of the system. When the pumping rate increases even further, the number of lasing modes no longer increases, but saturates to a constant value, which is proportional to the system size for a given randomness. This saturation is caused by spatial repulsion of lasing modes that results from gain competition and spatial localization of the lasing modes. This prediction was later confirmed experimentally (Ling *et al* 2001, Anni *et al* 2004). The time-dependent theory is especially suitable for the simulation of laser dynamics. Soukoulis *et al* simulated the dynamic response and relaxation oscillation in random lasers (Soukoulis *et al* 2002). The simulation reproduces most of the experimental observations and provides an understanding of the dynamic response of random lasers.

Vanneste and Sebbah calculate the spatial profile of lasing modes in 2D random media with the above method (Vanneste and Sebbah 2001, Sebbah and Vanneste 2002). They compare the passive modes of a 2D random system with the lasing modes when gain is activated. In the strong localization regime, the lasing modes are identical to the passive modes without gain. When the external pump is focused, the lasing modes change with the location of the pump, in agreement with the experimental observation. Therefore, local pumping of the system allows selective excitation of individual localized modes. Jiang and Soukoulis also show that knowledge of the density of states and the eigenstates of a random system without gain, in conjunction with the frequency profile of the gain, can accurately predict the mode that lases first when optical gain is added (Jiang and Soukoulis 2002).

The advantage of the time-dependent theory is that it can simulate lasing in a real random structure after inputting the structure and material information. The numerical simulation gives the lasing spectra, the spatial distribution of lasing modes and the dynamic response that can be compared directly with the experimental measurements. The problem is that simulation of large samples requires too much computing power and the running time is too long. So far, the numerical simulation have been carried out only in 1D and 2D systems, even though the method can be applied to 3D systems. Furthermore, the simulation must be done for thousands of samples with different configurations before any statistical conclusion can be drawn (Li *et al* 2001).

3.5. Quantitative dependence on scattering strength and pump area

The performance of a random laser depends critically on the scattering strength and pump area. A quantitative study is conducted on polymers doped with dye molecules and microparticles (Ling *et al* 2001). The microparticles serve as scattering centres and the excited dye molecules provide optical gain. The separation of scattering elements from gain medium allows the scattering strength be varied independently of the gain coefficient.

The random media in our experiment are PMMA sheets containing rhodamine 640 perchlorate dye and TiO₂ microparticles. The mean diameter of TiO₂ particles is 400 nm. The particle density is varied from 8×10^{10} to 6×10^{12} cm⁻³. The transport mean free path is characterized in the coherent backscattering experiment. l_t varies from 0.4 μm to 17 μm. The dye concentration is fixed at 5×10^{-2} M L⁻¹. In the lasing experiment, the dye molecules are optically excited by the second harmonics of a pulsed Nd:YAG laser. Figure 6(a) is a plot of the incident pump pulse energy at the lasing threshold versus the transport mean free path. As the TiO₂ particle density in the PMMA sheet increases, the transport mean free path decreases, so does the lasing threshold. The strong dependence of the lasing threshold on the transport mean free path confirms the essential contribution of scattering to lasing oscillation. With

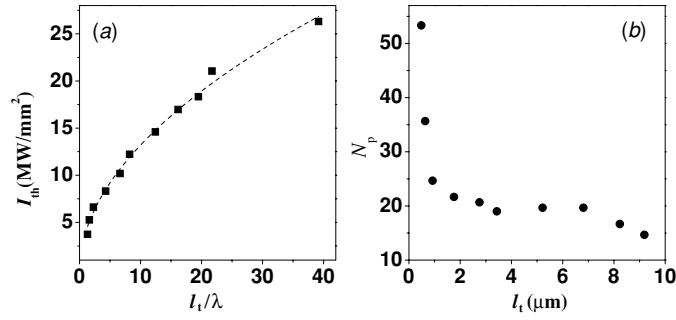


Figure 6. (a) The lasing threshold pump intensity I_{th} versus l_t/λ . The fitted curve (dashed line) is $I_{\text{th}} = 4.0(l_t/\lambda)^{0.52}$. (b) The number of lasing peaks N_p as a function of l_t at the fixed incident pump pulse energy $1.0 \mu\text{J}$.

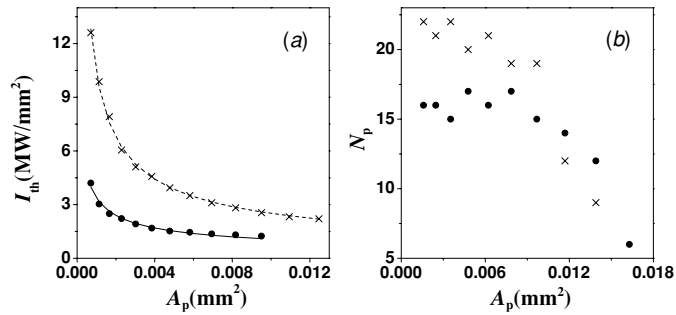


Figure 7. (a) The incident pump intensity at lasing threshold versus the area A_p of pump beam spot on the sample surface. l_t are $0.9 \mu\text{m}$ (circles) and $9 \mu\text{m}$ (crosses), respectively. The fitted curves are $I_{\text{th}} = 0.11A_p^{-0.5}$ (solid line) and $I_{\text{th}} = 0.15A_p^{-0.62}$ (dashed line). (b) The number of lasing modes versus the area of pump beam spot on the sample surface. $l_t = 0.9 \mu\text{m}$ (circles), $9 \mu\text{m}$ (crosses). The incident pump pulse energies are $0.63 \mu\text{J}$ and $1.0 \mu\text{J}$, respectively.

an increase in the amount of optical scattering, the feedback provided by scattering becomes stronger, thus the lasing threshold is reduced. Through curve fitting, we find that the lasing threshold pump intensity $I_{\text{th}} \propto l_t^{0.52}$. Figure 6(b) is a plot of the number of lasing peaks N_p versus l_t at a fixed pumping intensity. The shorter the transport mean free path, the more the lasing peaks emerge.

One interesting feature in figure 6 is that when the transport mean free path approaches the optical wavelength, the lasing threshold pump intensity drops quickly and the number of lasing modes increases dramatically. This result agrees with John and Pang's prediction of a dramatic threshold reduction in the regime $l_t \rightarrow \lambda$ of incipient photon localization (John and Pang 1996). Figure 6 also demonstrates lasing with resonant feedback in the diffusion regime $l_t \gg \lambda$. Despite the fact that the coherent feedback supplied by scattering is rather weak, lasing oscillation can still occur as long as the optical gain is high enough. However, tight focusing of pump light is necessary to observe discrete lasing peaks, e.g., the pump beam is focused to a $50 \mu\text{m}$ spot on the sample surface in figure 6. Hence, the gain volume is much smaller than that of the entire random medium, $L_g \ll L$.

Next, we investigate the dependence of lasing threshold and number of lasing modes on the pump area. In figure 7(a), the incident pump intensity at the lasing threshold I_{th} is plotted against the area A_p of pump beam spot on the sample surface. The data are collected from

two samples of $l_t = 0.9 \mu\text{m}$ and $9 \mu\text{m}$. In both samples, I_{th} decreases as A_p increases. Curve fitting reveals $I_{\text{th}} \propto A_p^{-q}$, where $q = 0.50, 0.62$ for $l_t = 0.9, 9 \mu\text{m}$, respectively. Figure 7(b) shows the number of lasing modes as a function of the pump area. In this measurement, the incident pump power is fixed while the pump area is varied. Thus, the incident pump intensity also changes with A_p . The number of lasing modes stays nearly constant when the diameter d_p of the pump spot increases from 50 to $110 \mu\text{m}$. Once $d_p > 110 \mu\text{m}$, the number of lasing modes starts decreasing quickly.

In order to understand the above experimental results, we need to find out how big the lasing modes are. Employing the spectrally resolved speckle analysis, we are able to map the spatial profile of individual lasing modes at the sample surface (Cao *et al* 2002). Experimentally, the far-field speckle pattern of one lasing mode is recorded, then Fourier-transformed to generate the spatial field correlation function in the near-field zone. Once above the lasing threshold, spatial coherence is established across the entire lasing mode. Hence, the spatial extent of the field correlation function directly reflects the mode size. We find that even in the diffusive samples, the lasing modes are not extended over the entire random medium; instead they are confined in the pumped region with an exponential tail extending out.

3.6. Spatial confinement of lasing modes by absorption

In a diffusive sample ($l_t \gg \lambda$), the quasimodes are expected to extend over the entire random medium. However, the experimental results demonstrate that the size of individual lasing modes is much smaller than that of the entire sample, indicating that the lasing modes are not extended states. Our earlier speculation was that the lasing modes correspond to some kind of anomalously localized states (Cao *et al* 2002). They are analogous to the prelocalized electronic states in diffusive conductors that are responsible for the long-time asymptotics of the current relaxation (Altshuler *et al* 1991, Fyodorov and Mirlin 1994, 1995, Falko and Efetov 1995a, 1995b, Mirlin 2000). Such states exhibit an anomalous build-up of intensity in a region of space. They are very rare in the diffusion regime. Note that the prelocalized states differ from the almost localized states in two aspects: (i) their size is larger than the transport mean free path; (ii) their properties are universal, in the sense that the disorder enters only via l_t . Since the number of prelocalized states is much less than that of the extended states in the diffusion regime, the transport properties are dominated by extended states. Therefore, it is hard to probe the prelocalized states in the transmission measurement. However, when optical gain is introduced to a random medium, the prelocalized states are preferably amplified because of their long lifetime. Photons in the prelocalized states stay longer in the gain medium, thus they experience more amplification. As optical gain increases further, the prelocalized states lase first because of their lower decay rates. Once the prelocalized states lase, their intensities are much higher than that of the extended states. Hence, they dominate the emission spectrum and the field pattern.

The anomalously localized states should be rare in the diffusive samples. Yet no matter where on the sample the pump beam is focused, we always observe lasing modes that are spatially confined in the vicinity of the pumped region. Moreover, the lasing threshold does not fluctuate much as the pump spot moves across the random medium. These experimental observations contradict the theory of anomalously localized states. Later, we realized that this discrepancy originates from the assumption that the lasing modes are the quasimodes of the passive random medium. Next, we demonstrate in a numerical simulation that this assumption is not valid when absorption at the emission wavelength is significant outside the gain volume.

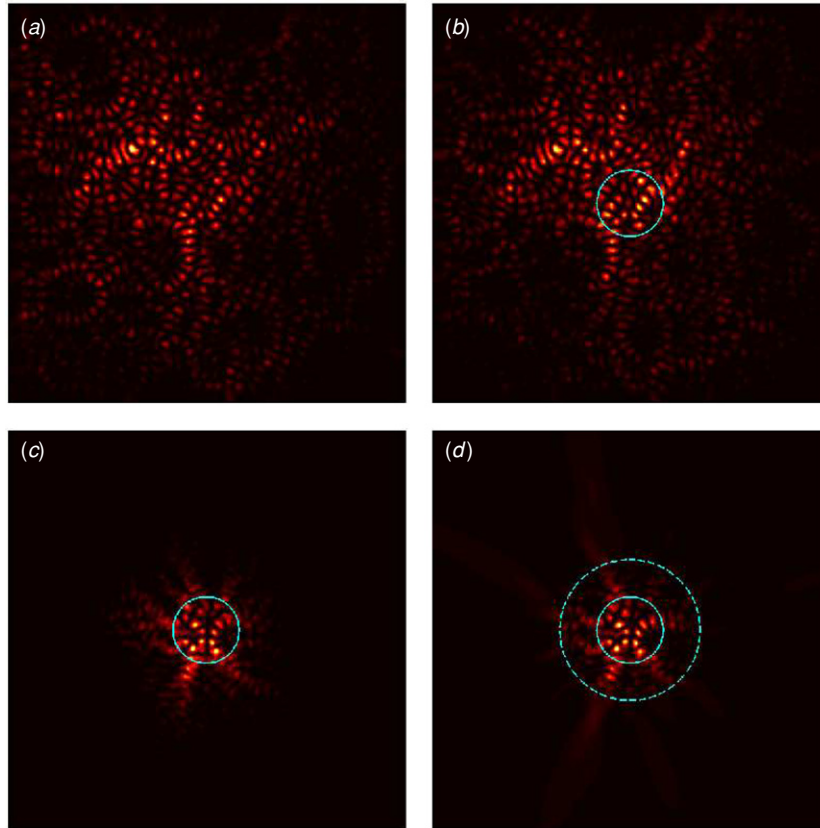


Figure 8. Calculated spatial intensity distribution of (a) the quasimode with the least decay rate in a passive diffusive system, (b) the (first) lasing mode with gain inside the circular region near the centre and no absorption outside it, (c) the (first) lasing mode with gain inside the circular region near the centre and absorption outside it, and (d) the (first) lasing mode with random medium beyond one l_{abs} (dashed circle) removed.

We use the FDTD method to simulate lasing in the transverse magnetic (TM) modes of 2D random media. Dielectric cylinders (diameter $d_c = 160$ nm, refractive index $n = 2$) are placed at random in vacuum with a filling fraction $\sim 50\%$. The total size of the system is $9.2 \mu\text{m} \times 9.2 \mu\text{m}$. The wavelength of interest $\lambda = 650$ nm. The numerical simulation of continuous wave (CW) transmission gives $l_t \simeq 1.3 \mu\text{m}$. Since $l_t/L \sim 0.12$ and $kl_t \sim 13$, light transport in this 2D system is diffusive.

We first calculate the quasimode with the least decay rate γ_{min} in the passive random medium. A short excitation pulse, whose spectrum is centred at $\lambda = 650$ nm, is launched in the centre of the sample. After the excitation pulse is gone, the total electromagnetic energy stored inside the random system $U(t)$ exhibits a non-exponential decay in time as a result of multimode excitation. However, after a sufficiently long time, $U(t)$ changes to an exponential decay because only one mode with the longest lifetime is left inside the system. The exponential decay rate of $U(t)$ is equal to γ_{min} . The spatial profile of the electric field becomes stable in time, and it reflects the wavefunction of this longest lived quasimode. For one realization shown in figure 8(a), the Fourier transform of electric field $E(t)$ gives the wavelength of the slowest decaying quasimode $\lambda = 646$ nm. Its

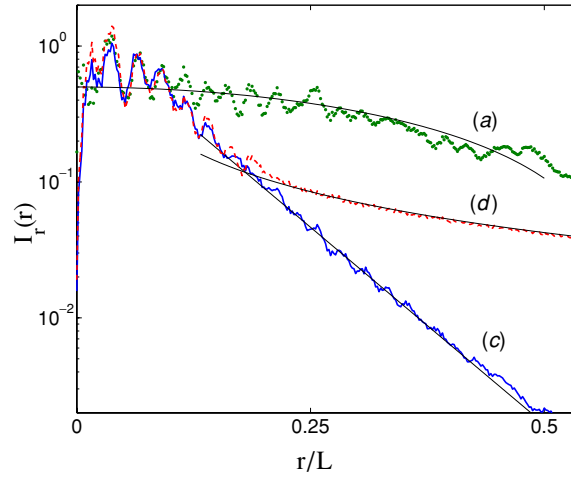


Figure 9. Radial dependence of the angularly integrated intensities of the modes (*a*, *c*, *d*) in figure 8. (*a*) is compared to the diffusive mode profile, the tail of (*c*) is fitted with an exponential decay and the fall-off of (*d*) outside the random medium is compared to r^{-1} .

intensity distribution reveals that this quasimode is extended across the sample. When some cylinders at the sample boundary are removed, the mode profile changes dramatically. The sensitivity of this quasimode to the boundary confirms that it is an extended state. Figure 9 shows the radial dependence of the angularly integrated intensity, $I_r(r) = \int |E(r, \theta)|^2 r d\theta$, where r is the radial coordinate, θ is the polar angle and $E(r, \theta)$ is the electric field distribution of the quasimode. For comparison, the radial profile of the lowest diffusion mode $\cos[\pi x/(L + 2z_0)] \cos[\pi y/(L + 2z_0)]$ is also plotted in figure 9. It describes $I_r(r)$ quite well.

Next, gain and reabsorption are introduced into the random medium. In the time-dependent theory presented in section 3.4, the gain medium is modelled as a four-level atomic system where the lasing transition is from level 2 to level 1. In the absence of pumping, all the atoms are assumed to be in level 0. Since the electronic population in level 1 is zero, there is no absorption at the lasing wavelength in the unpumped region. To simulate spatially non-uniform gain and reabsorption of laser emission, we use the semi-classical Lorentz model (Cao *et al* 2000b). The linear gain/absorption is modelled by negative/positive conductance. By introducing negative conductance to the pumped region and positive conductance to the unpumped region, we are able to describe both light amplification inside the pumped region and reabsorption of the emitted light outside the pumped region. More specifically, the cylinders have the conductance (Taflove and Hagness 2000)

$$\sigma(\omega) = \frac{\sigma_0/2}{1 + i(\omega - \omega_0)T_2} + \frac{\sigma_0/2}{1 + i(\omega + \omega_0)T_2}. \quad (12)$$

The sign of σ_0 determines light is amplified or absorbed, whereas the amplitude of σ_0 sets the magnitude of gain/absorption. ω_0 and $1/T_2$ determine the centre frequency and width of the gain/absorption spectrum, respectively. The absence of gain saturation in equation (12) is not crucial in our simulation, as our goal is to find the first lasing mode at or slightly above the lasing threshold. A seed pulse is launched at $t = 0$ to initiate the amplification process. The lasing threshold is defined by the minimum gain coefficient ($-\sigma_0$) at which the electromagnetic energy stored inside the random system grows continuously in time.

We simulate the case of local pumping without reabsorption outside the pumped region. For comparison, we use the same random sample as in figure 8(a) and introduce gain to the central part marked by the circle in figure 8(b). The gain spectrum is centred at 650 nm and has a width of 52 nm. The lasing mode shown in figure 8(b) is identical to the quasimode of the passive system in figure 8(a). Although optical gain is concentrated within the circle near the centre, the lasing mode is extended throughout the entire sample. As we reduce the pump area by decreasing the radius of the circle, the lasing threshold increases, but the lasing mode profile remains the same. This result indicates that the lasing mode in a diffusive random medium is identical to an extended quasimode of the passive system, even when the gain region is smaller than the mode size.

However, the above statement is valid only when there is no absorption outside the pumped region, which is not the case in most experiments. For example, rhodamine dye, which is widely used to provide gain for random lasers, has significant overlap between its absorption band and emission band. Therefore, photons that are emitted by the excited rhodamine molecules inside the pumped region may diffuse into the surrounding unpumped region and be absorbed by the unexcited rhodamine molecules there. The absorption reduces the probability of light returning to the pumped region, thus suppresses the feedback from the unpumped region. To simulate the reabsorption, we introduce absorption outside the pump area, the bulk absorption length (inelastic length) $l_i = 1.06 \mu\text{m}$. Figure 8(c) shows the lasing mode profile, which is very different from that in figure 8(a) or (b). The wavelength of the lasing mode also differs by about 4 nm. Therefore, the lasing mode in the presence of reabsorption is a new mode, completely different from the quasimode of the passive system. Due to reabsorption outside the pump area, the lasing mode is confined more or less inside the pumped region. The radial profile of the lasing mode, shown in figure 9, features an exponential decay outside the pumped region. The decay length, $\sim 0.8 \mu\text{m}$, is equal to the absorption length $l_{\text{abs}} = (l_i l_i / 2)^{1/2}$. To confirm this result, we simulate transmission of CW plane wave through a slab of disordered absorbing medium and obtain the same attenuation length.

The observed effect indicates that reabsorption, which suppresses the feedback from the unpumped part of the sample, effectively reduces the system size. To check this conjecture, we remove all the random medium beyond one l_{amp} from the pump area (dashed circle in figure 8(d)) and repeat the calculation. The frequency and spatial profile of the lasing mode remain the same (figure 8(d)), despite the drastic change of the random system. The radial profile of the lasing mode outside the random medium (figure 9) exhibits a trivial r^{-1} dependence. This result indicates that the lasing mode is an extended state within the effective region of dimension $L_{\text{eff}} \sim L_g + l_{\text{abs}}$. It is fundamentally different from the quasimode of the passive system. Even if all the quasimodes of a passive diffusive system are extended across the entire sample, the lasing modes are still confined in the pumped volume with an exponential tail outside it.

The above conclusion can be applied to 3D diffusive random media and explain the experimental results qualitatively. When the pump beam is tightly focused, the effective system volume is reduced due to reabsorption of emission outside the pumped region. It leads to a decrease of the Thouless number $\delta \propto L_{\text{eff}}$, as $\delta \nu \propto L_{\text{eff}}^{-2}$ and $\nu \propto L_{\text{eff}}^{-3}$. The smaller the value of δ , the larger the fluctuation of the decay rates γ of the quasimodes (Chabanov *et al* 2003). The variance of the decay rates $\sigma_\gamma^2 = \langle \gamma \rangle^2 / \delta$ (Mirlin 2000), thus $\sigma_\gamma / \langle \gamma \rangle \propto L_{\text{eff}}^{-1}$. We believe that the broadening of the decay rate distribution along with the decrease of the total number of quasimodes (within the effective volume) is responsible for the observation of discrete lasing peaks in the tight focusing condition. Despite its value being reduced, the effective Thouless number is still much larger than 1 because of weak scattering. As a result,

the lasing modes are the extended states within the effective volume. Because $\sigma_\gamma/\langle\gamma\rangle \ll 1$, the minimum decay rate γ_{\min} is still close to $\langle\gamma\rangle$, leading to a relatively small fluctuation of lasing threshold. The threshold gain can be estimated as $g_{\text{th}} = \gamma_{\min} \approx \langle\gamma\rangle \sim D/L_{\text{eff}}^2$. This estimation gives a threshold equal to that predicted by Letokhov for random lasing with non-resonant feedback (Letokhov 1968), $l_{\text{amp}} \sim L_{\text{eff}}$ or $l_{\text{g}} \sim L_{\text{eff}}^2/l_{\text{t}}$. Using this approximation and taking into account the saturation of absorption of pump light, we are able to explain the measured dependence of the lasing threshold pump intensity I_{th} on l_{t} and the pump area A_{p} , i.e. $I_{\text{th}} \propto l_{\text{t}}^{1/2}/A_{\text{p}}^q$, where $0.5 \leq q \leq 1$ (Burin *et al* 2003a). We also understand qualitatively why the shot-to-shot fluctuation of lasing peaks gets stronger in weaker scattering samples. When the scattering is weak, $P(\gamma)$ is narrow, thus there are many modes with similar decay rates. Which states would lase in one shot (pump pulse) depends on the initial noise (spontaneous emission). Therefore, the lasing peaks in different shots may not be the same.

We comment that our model does not contradict the theory of anomalously localized states, in the sense that it does not eliminate the possibility of rare events. The anomalously localized states, despite rare, do exist in the diffusive samples (Uski *et al* 2000, 2001, Nikolić 2001, Ossipov *et al* 2002, 2003, Kottos *et al* 2003, Weiss *et al* 2005). If they happen to be *within* the pumped volume, the anomalously localized states could serve as low-threshold lasing modes. However, even in the absence of such rare events, the interplay between optical amplification and reabsorption could result in spatial localization of lasing modes in the pumped region. In other words, local pumping in an absorbing medium generates a local ‘potential well’ to trap the lasing modes.

The above conclusion applies not only to the diffusion regime, but also to the localization regime. If the size of gain volume is smaller than that of localized states *and* strong absorption exists outside the pumped region, the lasing modes differ from the localized states in the passive system.

4. One-dimensional photon localization laser

4.1. Experimental realization

One problem of the 3D random lasers described in the previous sections is that multiple scattering of pump light restricts the excitation to the proximity of sample surface. The emitted photons readily escape through the sample surface, giving a high lasing threshold. This problem is less serious in 2D random lasers, as the pump light incident from the third dimension does not experience scattering (Stassinopoulos *et al* 2005). Yet the pump light is not confined inside the 2D random system. Recently, Milner and Genack have realized photon localization laser in which the pump light is localized deep inside a one-dimensional (1D) random structure (Milner and Genack 2005).

The 1D sample is a stack of partially reflecting glass slides of random thickness between 80 and 120 μm with interspersed dye films. The stack is illuminated at normal incidence by the second harmonics of a pulsed Nd:YAG laser. In this 1D structure, light is localized by multiple scattering from the parallel layers which returns the wave upon itself. The average transmittance through a stack of glass slides without intervening dye solution decays exponentially with the number of the slides. Even though the average transport of light is suppressed, resonant tunnelling through localized states gives spectrally narrow transmission peaks. A large number of narrow peaks are observed in the transmission spectra. When the pump wavelength is tuned into one of the narrow transmission lines, the pump light penetrates deep into the sample’s interior via resonant excitation of a long-lived spatially localized mode. Energy absorbed from this mode is subsequently emitted into long-lived localized modes

which fall within the dye emission spectrum. Stimulated emission is enhanced when the spatial energy distributions at both the excitation and emission wavelengths overlap. The deposition of pump energy deep within the sample and its efficient coupling to long-lived emission modes removes a major barrier to achieving low-threshold lasing in the presence of disorder. The threshold is sufficiently low for lasing to be induced with a quasi-continuous illumination by a 3 W argon-ion laser.

Another feature of the 1D photon localization laser is the large fluctuation in lasing power when the pump beam is focused onto different parts of the sample which correspond to different realizations of disorder. The pump transmission is strongly correlated with the output lasing power. High pump transmission results from resonant excitation of a localized mode which is spatially peaked near the centre of the sample. Therefore, the pump energy is exponentially enhanced within the sample and is efficiently transferred to the gain medium. Since excitation in the centre of the sample is likely to escape via emission into localized modes with long lifetime, the opportunity for stimulated emission is enhanced and the laser output is high.

4.2. Analytical model

Analytical approaches have been taken to derive the conditions for coherent steady-state lasing oscillation in 1D random media (Herrmann and Wilhelm 1998, Burin *et al* 2002, Jiang and Soukoulis 2002). In analogy to a Fabry-Perot cavity laser, the threshold conditions for coherent lasing in a 1D random system include both the steady-state round-trip gain condition and the round-trip phase shift condition.

According to the semiclassical laser theory, the Maxwell equation for the electric field $E(x, t)$ in a 1D random system is

$$\nabla^2 E(x, t) + \mu_0 \sigma \frac{\partial E(x, t)}{\partial t} + \mu_0 \varepsilon(x) \frac{\partial^2 E(x, t)}{\partial t^2} = -\mu_0 \frac{\partial^2 P_g(x, t)}{\partial t^2}. \quad (13)$$

The dielectric constant $\varepsilon(x)$ is determined by the random configuration of dielectric layers. The permeability of a dielectric medium at optical frequency is nearly equal to that in vacuum, $\mu \simeq \mu_0$. σ represents the loss due to light absorption and leakage out of the system. The leakage loss can be expressed as $\varepsilon_0 \omega / Q$, where Q is the quality factor. P_g is the polarization induced by gain. The slowly varying approximation gives $E(x, t) = E_0(t) \phi(x) \exp(-i\omega t)$, where $E_0(t)$ is the field amplitude, $\phi(x)$ is the normalized field distribution and ω is the frequency of field oscillation. The real and imaginary parts of equation (13) give (Jiang and Soukoulis 2002)

$$\nabla^2 \phi(x) + \mu_0 [\varepsilon(x) + \varepsilon_0 \chi'(x, \omega)] \omega^2 \phi(x) = 0, \quad (14)$$

$$\frac{dE(t)}{dt} = \left(-\langle \chi''(\omega) \rangle - \frac{1}{Q} \right) \frac{\varepsilon_0 \omega E(t)}{2\langle \varepsilon \rangle}, \quad (15)$$

where $\langle \varepsilon \rangle = \int_0^L \varepsilon(x) dx / L$ is the spatially averaged dielectric constant inside the system and $-\langle \chi'' \rangle = -\int_0^L \phi(x)^* \chi''(x, \omega) \phi(x) dx / L$ represents the spatially averaged gain that takes into account the overlap between the field distribution and the active region.

Equation (14) determines the lasing frequency ω , the field distribution $\phi(x)$ and the quality factor Q . The term $\varepsilon_0 \chi'(x, \omega)$ causes a shift of the lasing frequency from the eigenfrequency of the passive system, that is the pulling effect. For a localized mode, $Q \gg 1$, a small gain is needed to reach the lasing threshold. Then, $\chi'(x, \omega) \ll 1$, the pulling effect is very weak. The lasing frequency is almost the same as the eigenfrequency of the passive system and the field distribution is nearly identical to the eigenfunction of the passive system. Equation (15) is a time-dependent equation for the field amplitude; it sets the threshold $-\langle \chi''(\omega) \rangle = 1/Q$ for

lasing oscillation. When the gain is over threshold, $E_0(t)$ builds up in time. The population inversion ΔN gets depleted, leading to a decrease of χ'' until $-\langle\chi''(\omega, E_0)\rangle = 1/Q$. Then, the field amplitude becomes stable in time.

In the localization regime, the sample length L is much larger than the localization length ξ . If the gain is uniform throughout the 1D structure, the first lasing mode is usually the most localized mode in the middle of the random structure. Let us consider such a mode located at $x_0 \sim L/2$. The random media on its left side and right side are characterized by the reflection coefficients (r_l, r_r) and transmission coefficients (t_l, t_r). The threshold gain g_{th} is related to the reflection coefficients (Burin *et al* 2002):

$$|r_l r_r| \exp[g_{\text{th}}(d\Phi_l/d\omega + d\Phi_r/d\omega)/2] = 1, \quad (16)$$

where $r = |r| e^{i\Phi}$. The frequency dependence of $|r|$ can be neglected because $L \gg \xi$ and $1 - |r| \ll 1$. The factor in the exponent of equation (16) represents a product of photon amplification rate and the trapping time of photons inside the system $\tau_0 = d\Phi_l/d\omega + d\Phi_r/d\omega$. Since $|r_l|$ and $|r_r|$ are very close to 1, g_{th} can be expressed in terms of the transmission coefficients with the linear expansion

$$g_{\text{th}} \approx \frac{|t_l|^2 + |t_r|^2}{d\Phi_l/d\omega + d\Phi_r/d\omega}. \quad (17)$$

In the localization regime, $t_l \sim \exp(-x_0/\xi)$, $t_r \sim \exp[-(L - x_0)/\xi]$. Hence, $g_{\text{th}} \sim \{\exp(-2x_0/\xi) + \exp[-2(L - x_0)/\xi]\}/\tau_0$. Since $x_0 \sim L/2$, $g_{\text{th}} \propto \exp(-L/\xi)$, the lasing threshold depends exponentially on the system length L . The photons emitted inside the random system need an exponentially long time to escape from it, due to exponentially small transmission in the localization regime. Therefore, an exponentially small gain is enough to initiate lasing oscillation.

5. Quantum theory of random lasers

5.1. Photon statistics of random lasers with non-resonant feedback

The development of quantum theory on a random laser started in the 1960s when Letokhov and co-workers investigated the statistical properties of emission from a laser with a scattering reflector (Ambartsumyan *et al* 1967, 1968, 1970). In their laser, one mirror of the Fabry-Perot cavity is replaced by a scattering surface. Light in the cavity undergoes multiple scattering, its propagation direction or wave vector being changed constantly. Thus, the modes, defined by the wave vectors, interact strongly via radiation exchange by scattering. Lasing occurs simultaneously in a large number of modes with different wave vectors. In the master equations for photon probability distribution in each mode, they added terms that phenomenologically describe the linear interaction of modes through scattering. Their theoretical and experimental studies lead to two conclusions. (i) The number of photons in a single lasing mode is subject to strong fluctuations, and its distribution coincides with the Bose-Einstein distribution of black-body radiation. (ii) The total number of photons in all lasing modes exhibits a fluctuation much smaller than that of the black-body radiation in the same number of modes. Well above the lasing threshold, gain saturation quenches the total photon number fluctuation, yet it fails to stabilize the photon number in a single mode due to frequent hopping of photons from one mode to another. That is why the photon number distribution in a single lasing mode is similar to that of non-coherent source.

Recently, Florescu and John have developed the master equation formalism to random lasers with non-resonant feedback (Florescu and John 2004a, 2004b). A diffusive random medium is partitioned into a collection of hypothetical cells of dimension l_c . Each cell is

labelled by a coarse-grained position vector \mathbf{r} . Since $l_t \gg \lambda$, it is possible to associate a mode with the approximate position \mathbf{r} and wave vector \mathbf{k} . In a random laser with non-resonant feedback, all modes within the pumped region contribute equally on average to the overall lasing process. Florescu and John generalize the master equations for conventional lasers by replacing the cavity loss terms with diffusion terms that describe the multiple scattering character of light transport. This description attributes feedback to average wave transport that leads to lasing throughout the entire medium. By summing over \mathbf{k} , they obtain the master equations for photon probability distribution in each cell \mathbf{r} . These equations allow evaluation of the average emission coherence at different positions inside the random medium. They find that deeper inside the sample, the Fano–Mandel parameter gets smaller. This result indicates that the photon number fluctuation in the cells deep inside the sample is quenched, despite exchange of photons among neighbouring cells.

5.2. Excess noise of amplified spontaneous emission

Using the Green functions to directly quantize the wave equation, Beenakker and co-workers have established a general relation between the emission from a linear optical medium and the underlying scattering matrix (Beenakker 1998, Patra and Beenakker 1999, Mishchenko *et al* 2001). A random medium, with linear gain or absorption, is coupled to the environment via N channels at frequency ω . The input and output fields are represented by two N -component vectors of annihilation operators $a_{\text{in}}(\omega)$ and $a_{\text{out}}(\omega)$. The input–output relation takes the form

$$a_{\text{out}} = Sa_{\text{in}} + Ub + Vc^\dagger, \quad (18)$$

where S is the $N \times N$ scattering matrix, b and c^\dagger describe absorbing and amplifying media. Beenakker obtained the general relation (Beenakker 1998)

$$UU^\dagger - VV^\dagger = 1 - SS^\dagger. \quad (19)$$

It can be understood as a fluctuation–dissipation relation: the left-hand side accounts for quantum fluctuations in the electromagnetic field due to spontaneous emission or absorption of photons, and the right-hand side accounts for dissipation due to absorption or amplification due to stimulated emission. Equation (19) represents a powerful link between the classical optics described by the scattering matrix S and the quantum optics represented by the quantum fluctuation matrices U, V . Combining this relation with the statistical properties of the scattering matrix in disordered media, Beenakker derived the full photocount distribution of the radiation emitted from random media with linear gain (Beenakker 1998). The amplified spontaneous emission exhibits excess noise below the lasing threshold. The origin of this excess noise lies in the presence of a large number of overlapping modes and a broad distribution of the corresponding scattering strengths.

5.3. Quantum theory of random laser with non-overlapping modes

The scattering matrix approach cannot be applied to random laser above the threshold, as it does not include the saturation effects of the medium. To describe photon statistics above the lasing threshold, Patra has developed a theory that includes the nonlinear effect of gain saturation (Patra 2002). Noise is described by Langevin terms, where fluctuations of both the electromagnetic field and the active medium are included. His theory is valid only for random lasers with small outcoupling, i.e. the quasimodes do not overlap in frequency (non-overlapping modes). Since a large number of modes can be above lasing threshold simultaneously (Misirpashaev and Beenakker 1998), mode competition for optical gain

introduces additional noise. The amount of photon number fluctuation in each lasing mode is increased above the Poissonian value by an amount that depends on the number of lasing modes.

Taking a different approach, Peřinová *et al* consider the master equation in the Linblad form for a random laser with non-overlapping modes (Peřinová *et al* 2004). They derive the rate equations for the probability distributions as well as the equations for the means and moments. Based on the open system theory, a new form of the Fano factor is proposed to describe the photon statistics of a random laser.

5.4. Field quantization for open chaotic resonator with overlapping modes

The quantum theory for random laser with non-overlapping modes can be applied to the photon localization regime where the Thouless number $\delta \leq 1$, but not the diffusion regime where $\delta > 1$. The first step in the development of quantum theory for random laser with coherent feedback in a random medium of $\delta > 1$ is to quantize the electromagnetic field in such an open system. Standard field quantization theory applies to cavities that are closed or nearly closed ($\delta < 1$). Hackenbroich *et al* have developed a quantization scheme for optical resonators with overlapping modes ($\delta > 1$). They employ the Feshbach's projector technique to quantize the electromagnetic field with arbitrary polarization. The field Hamiltonian of an open resonator with $\delta > 1$ reduces to the well-known system-and-bath Hamiltonian of quantum optics.

$$H = \sum_{\beta} \hbar \omega_{\beta} a_{\beta}^{\dagger} a_{\beta} + \sum_m \int d\omega \hbar \omega b_m^{\dagger}(\omega) b_m(\omega) + \hbar \sum_{\beta, m} \int d\omega [W_{\beta m}(\omega) a_{\beta}^{\dagger} b_m(\omega) + V_{\beta m}(\omega) a_{\beta} b_m(\omega) + \text{h.c.}]. \quad (20)$$

a_{β} is the annihilation operator of photons in the β th mode inside the resonator, and likewise $b_m(\omega)$ is that of photons in the (m, ω) th mode outside the resonator. $W_{\beta m}$ and $V_{\beta m}$ describe the couplings between the inside modes and outside modes. The continua of outside modes act as a 'bath' damping the discrete inside modes. When the bath degrees of freedom are eliminated, the dynamics of the inside modes becomes irreversible. The Heisenberg equations of motion for the inside amplitudes a_{β} take the form of Langevin equations, in which the outside amplitudes $b_m(\omega), b_m^{\dagger}(\omega)$ enter only with their initial values in the Langevin noise forces. If the anti-resonant terms are neglected and the Markovian approximation is taken, the Langevin equations for a_{β} can be simplified as

$$\dot{a}_{\beta}(t) = -i\omega_{\beta} a_{\beta}(t) - \pi \sum_{\beta'} [W W^{\dagger}]_{\beta\beta'} a_{\beta'}(t) + F_{\beta}(t), \quad (21)$$

where the noise operator $F_{\beta}(t) = -i \int d\omega e^{-i\omega(t-t_0)} \sum_m W_{\beta m} b_m(\omega, t_0)$. The inside mode operators a_{β} are coupled by the damping matrix $W W^{\dagger}$. As different inside modes couple to the same outside modes, the noise operators F_{β} are correlated, $\langle F_{\beta}^{\dagger} F_{\beta'} \rangle \neq \delta_{\beta\beta'}$. The mode coupling by both damping and noise can be understood as a consequence of the fluctuation-dissipation theorem. The mode dynamics of open chaotic resonators is determined not only by the eigenvalues of the internal Hamiltonia, but also by the coupling strength to the external radiation field. Therefore, the spectrum of such resonators is governed by a non-Hermitian random matrix. The master equations for the reduced density operator $\rho(t)$ of the inside field are also derived in the Schrödinger picture (Hackenbroich *et al* 2003). It is proven to be equivalent to the Langevin equation for a_{β} . The next step would be to incorporate the

amplifying medium into such an open resonator to simulate a random laser with overlapping modes.

6. Interplay of light localization and coherent amplification

Without a counterpart in the electronic system, the coherent amplification of light adds a new dimension to the fundamental study of mesoscopic wave transport. The interplay between light localization and coherent amplification has attracted much interest. It is well known that optical absorption hinders photon localization as it suppresses the interference effect of scattered light. Optical amplification enhances the interference phenomena in random media, thus it facilitates light localization. However, the criterion for Anderson localization of light in an amplifying random medium remains to be developed. The very concept of describing the Anderson localization transition in terms of a vanishing diffusion coefficient as an order parameter, familiar from systems with energy or particle number conservation, becomes questionable in active or dissipative media, where another channel for change of the energy density exists besides diffusion (Lubatsch *et al* 2005). A few years ago, a new criterion was developed for photon localization in passive and dissipative random media (Chabanov *et al* 2000). Chabanov, Stoychev and Genack demonstrate that the variance of transmission fluctuation accurately reflects the extent of localization even in the presence of absorption. Unfortunately, this criterion does not seem to hold for active random media, because the variance of transmission fluctuation would diverge at the lasing threshold. Gain saturation prevents this divergence, but the actual value of transmission variance depends on the saturation intensity which is determined by the material properties instead of wave transport. There is also doubt in applying the Thouless criterion for light localization in a passive random system to an active system. The ensemble-averaged spectral correlation function is dominated by the rare lasing configurations, thus the spectral correlation width $\delta\nu$ is equal to the lasing linewidth which also depends on the properties of gain material. Despite of the ambiguity in determining light localization in active random systems, there have been many studies on how coherent amplification affects light transport in disordered media.

The modification of coherent backscattering (weak localization) by amplification is investigated both theoretically (Zyuzin 1994, Deng *et al* 1997, Tutov and Maradudin 1999) and experimentally (Wiersma *et al* 1995b, de Oliveira *et al* 1996). The shape of the backscattering cone is determined by the transport distance of light in the medium. The intensity in an amplifying medium grows exponentially with the path length. Consequently, gain enhances the long path length that constitute the top of the backscattering cone. A relatively larger contribution of long paths yields a sharper and narrower cone as compared to the passive medium.

The effects of amplification on light reflection and transmission in a random system are extensively studied and compared with the effect of absorption (Pradhan and Kumar 1994, Zhang 1995, Zyuzin 1995, Beenakker 1996, Paasschens *et al* 1996, Burkov and Zyuzin 1996, 1997, Freilikher *et al* 1997, Joshi and Jayannavar 1997, Jiang and Soukoulis 1999, Jiang *et al* 1999, Ramakrishna and Kumar 2000, Ramakrishna *et al* 2000, Kumar 2001). These studies are carried out mostly in a 1D or quasi-1D system with the time-independent theory. Optical gain is introduced through the imaginary part of the refractive index. Below the lasing threshold, coherent amplification enhances light reflection and suppresses light transmission. It also leads to an increase in the fluctuation of the transmissivity T and reflectivity R . On approaching the lasing threshold, both the mean value and the variance of T and R diverge. Above the lasing threshold, random amplifier becomes a random oscillator with self-sustaining

oscillations in the quasimodes of the system. The time-independent theory no longer works, and it is replaced by the time-dependent theory that takes into account gain saturation.

6.1. Effects of amplification on field and intensity correlations

In a passive random system, nonlocal intensity correlation reflects the closeness to Anderson localization transition (Berkovits and Feng 1994, van Rossum and Nieuvenhuizen 1999). Light transport in an amplifying random medium experiences enhanced contribution from long paths, that should have a profound effect on the nonlocal intensity correlation. We investigate the local and nonlocal correlations of light transmitted through active random media (Yamilov and Cao 2005).

Due to formal similarity, it is tempting to treat a random system with gain as if it had ‘negative absorption’ and directly adopt the results obtained for a dissipative system. Such simplistic approach to correlation functions is fundamentally flawed. Theoretically, the spatial and spectral correlation functions are obtained by average over an infinite number of random realizations. Among them, there exist rare configurations containing anomalously localized states that could lase in the presence of small gain. Light intensity in the lasing configurations diverges, so do the ensemble-averaged correlation functions. Despite the divergence is prevented by gain depletion, the lasing configurations have much higher intensity than the non-lasing ones, thus they dominate the correlation functions. The width of spectral correlation functions is simply equal to the lasing mode width, while the spatial correlation functions only reflect the spatial profile of the lasing modes. This is in contrast to the ‘negative absorption’ model, which does not contain the divergent contribution of the rare events. In order to obtain the correlation functions that reflect light transport in amplifying random media, we introduce the conditional average over all non-lasing configurations $\langle \dots \rangle \rightarrow \langle \dots \rangle_c$. Such replacement, together with the fact that the fraction of lasing configurations varies with the amount of gain, makes any analytical derivation challenging. Numerical simulation turns out to be a fruitful alternative.

We introduce a numerical method of studying correlation functions based on the FDTD algorithm. This method allows us to solve the time-dependent Maxwell equations for the electromagnetic field at any point inside and outside a random medium. It makes no approximation about the scattering strength, accounts for all interference phenomena and gives correlation functions in both diffusion and localization regimes (Chang *et al* 2004). Optical gain can be incorporated into the Maxwell equations as a negative conductivity. For the study of amplification effect on light transport, numerical simulation has two advantages over real pump-probe experiments: (i) optical gain can be introduced uniformly across the entire random medium; (ii) coherent amplification of an input signal is easily separated from spontaneous emission of the active medium.

The FDTD method allows simulation of any real random structure. As an example, we consider a quasi-1D system with parameters close to the microwave experiments performed in Genack’s group (Sebbah *et al* 2002). To shorten the computation time, we simulate 2D random medium instead of 3D random medium in a waveguide geometry. As shown in the inset of figure 10(a), circular dielectric scatterers (refractive index = 2, diameter = 1.4 cm) are randomly positioned in a metallic waveguide. The metallic walls of the waveguide ensure 99.9% reflectivity. The waveguide width w is between 20 and 40 cm. Since the wavelength of interest $\lambda \sim 2$ cm, the number of waveguide channels $N_c = 2w/\lambda \sim 20-40$. In this quasi-1D system, the localization length $\xi = N_c l_t$. When the length of random medium L is smaller than ξ but larger than l_t , light transport is diffusive. The transition from diffusion to localization can be realized by increasing L to over ξ . We define $g_o \equiv (\pi/2)n_e N_c l_t / L'$,

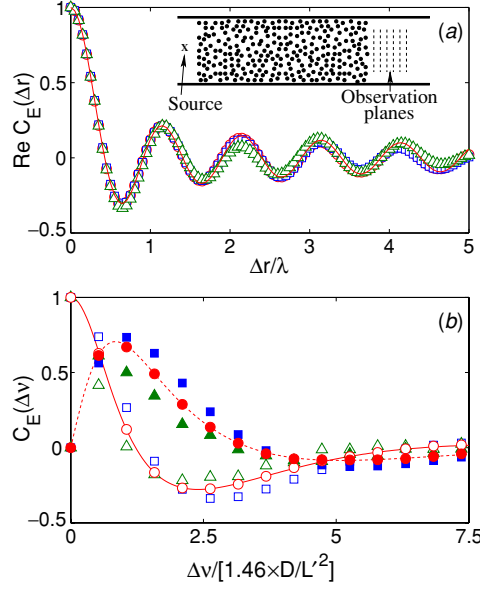


Figure 10. (a) Real part of $C_E(\Delta r)$; (b) real (open symbols, solid line) and imaginary (solid symbols, dashed line) parts of $C_E(\Delta \nu)$. Circles, squares and triangles represent the numerical data for passive ($\tau_{\text{abs/amp}} = \infty$), absorbing ($\tau_{\text{abs}} = -5\tau_{\text{amp}}^{\text{cr}}$) and amplifying ($\tau_{\text{amp}} = 5\tau_{\text{amp}}^{\text{cr}}$) systems, respectively. $L = 40$ cm, $w = 20$ cm, $l_t = 0.18$ cm. Curves represent theoretical fit with $z_b/l_t = 0.8$. The inset is a sketch of the numerical experiment.

where $L' = L + 2z_b$, z_b is the extrapolation length, $n_e = c/v_e$, v_e is the energy transport velocity. In the absence of gain or absorption, g_o is equal to the dimensionless conductance g_c when $g_c \gg 1$. To demonstrate the independence of our results on microscopic structure of the random medium, we vary both the filling fraction of scatterers and the length of the random medium to obtain samples with g_o between 2.2 and 9.0. The effect of gain or absorption (inside the scatterers) is treated by the classical Lorentzian model with positive or negative conductivity. In the numerical experiment, a TM-polarized broadband pulse centred at $\lambda = 2$ cm is launched via a point source at the input end of the waveguide. Temporal discrete Fourier transform is applied to the electric fields at the output end. By virtue of the discrete Fourier transform, we obtain the CW response of the system for a number of wavelengths. We calculate the ensemble-averaged correlation functions for the field

$$C_E(\Delta r, \Delta \nu) \equiv \frac{\langle E(\mathbf{r} + \Delta \mathbf{r}, \nu + \Delta \nu) E^*(\mathbf{r}, \nu) \rangle}{\langle I(\mathbf{r} + \Delta \mathbf{r}, \nu + \Delta \nu) \rangle^{1/2} \langle I(\mathbf{r}, \nu) \rangle^{1/2}} \quad (22)$$

and intensity

$$C(\Delta r, \Delta \nu) \equiv \frac{\langle I(\mathbf{r} + \Delta \mathbf{r}, \nu + \Delta \nu) I(\mathbf{r}, \nu) \rangle}{\langle I(\mathbf{r} + \Delta \mathbf{r}, \nu + \Delta \nu) \rangle \langle I(\mathbf{r}, \nu) \rangle} - 1, \quad (23)$$

at the output end. In the presence of gain, long after the short excitation pulse, the electromagnetic field decays with time in the non-lasing realizations, while it keeps increasing in the lasing ones. We exclude the lasing realizations from the ensemble average for correlation functions.

Based on the pairing of incoming and outgoing channels, three contributions to intensity correlation function have been identified (Berkovits and Feng 1994, van Rossum and Nieuvenhuizen 1999): a local (short-range) $C_1 \approx |C_E|^2$, and two nonlocal C_2 (long-range)

and C_3 (infinite-range) ones. For diffusive transport ($g_o \gg 1$) in a waveguide geometry, $C_1 \sim 1$, $C_2 \sim 1/g_o$ and $C_3 \sim 1/g_o^2$, making the values of C_2 and C_3 small. The nonlocal terms are brought about by long propagation paths which are most sensitive to the effect of amplification. As will be shown next, the nonlocal correlations are greatly enhanced by coherent amplification.

The spatial field correlation function in 3D bulk random media is originally derived by Shapiro (1986). Later, Freund and Eliyahu calculate it at the output surface of a 3D random medium (Freund and Eliyahu 1992). Similarly, we derive the corresponding expression in the 2D case (Chang *et al* 2004):

$$C_E(\Delta r) = \frac{\pi(z_b/l_t)J_0(k\Delta r) + 2\sin(k\Delta r)/k\Delta r}{\pi z_b/l_t + 2}, \quad (24)$$

where J_0 is the zeroth-order Bessel function. The imaginary part of $C_E(\Delta r)$ should vanish due to isotropy (Sebbah *et al* 2000), which is confirmed by our calculation where its value is less than 10^{-3} . The real part of $C_E(\Delta r)$ is found unchanged in the presence of gain or absorption, as shown in figure 10(a) for a system of $g_o = 2.2$. Equation (24) gives an excellent fit for passive, absorbing and amplifying systems with the same value of z_b/l_t . Physically, this invariance can be explained by the local nature of $C_E(\Delta r)$. Spatial field correlation contains information that comes from the length scale of transport mean free path. l_t is always shorter than the gain length l_g : $l_g/l_t > (2n_e/\pi^2) \cdot (L'/l_t)^2 \gg 1$, because the system is below the diffusive lasing threshold ($L' < \pi l_{\text{amp}}$). Since amplification occurs on the scale much longer than l_t , it has negligible effect on short-range transport and local spatial correlations.

The spectral field correlation function $C_E(\Delta\nu)$ contains an important dynamical parameter of transport—the diffusion coefficient $D = v_e l_t/2$. The spectral correlation width $\delta\nu$ is defined as the width at half maximum of $|C_E(\Delta\nu)|^2$ divided by a numerical factor 1.46. In a passive system, $\delta\nu$ is equal to the average mode linewidth D/L^2 . Since v_e can be determined separately through calculation of energy distribution between air and dielectric scatterers, the transport mean free path is found by fitting of the real and imaginary parts of $C_E(\Delta\nu)$ (figure 10(b)). The value of l_t allows us to calculate g_o . In the presence of absorption, the numerically calculated $C_E(\Delta\nu)$ fits well the expression derived in Pnini and Shapiro (1991), Kogan and Kaveh (1992) and van Rossum and Nieuvenhuizen (1993). In the case of amplification, we obtain the ‘negative absorption’ formula by replacing the absorption time $\tau_{\text{abs}} = l_{\text{abs}}/v$ with the negative amplification time $-\tau_{\text{amp}} = -l_{\text{amp}}/v$:

$$C_E(\Delta\nu) = \frac{\sinh(q_0 a) \sin(L'/l_{\text{amp}})}{\sinh(q_0 L') \sin(a/l_{\text{amp}})}, \quad (25)$$

where $q_0 = \gamma_+ - i\gamma_-$, $\gamma_{\pm}^2 = (\sqrt{1/l_{\text{amp}}^4 + \beta^4} \mp 1/l_{\text{amp}}^2)/2$, $\beta = \sqrt{2\pi\Delta\nu/D}$ and the randomization length $a \simeq l$. By fitting $C_E(\Delta\nu)$ with equation (25), we obtain $\delta\nu$, which is plotted in figure 11 for systems of $g_o = 4.4$ and 9.0. The narrowing of spectral correlation width by gain is due to partial compensation of light leakage through the system boundary. Absorption, in contrast, introduces an additional loss mechanism, that leads to an increase of $\delta\nu$. For both amplifying and absorbing media, the calculated $\delta\nu$ agrees well with the diffusion prediction. This agreement in the case of amplification is unexpected. The ‘negative absorption’ theory neglects the fluctuation of lasing threshold and assumes that the spectral width of all modes decreases with gain uniformly. However, the width γ of quasimodes has a distribution $P(\gamma)$, schematically plotted in the inset of figure 11. For a given amount of gain, the modes with small γ in the tail (Ω_1) of $P(\gamma)$ lase, and they are excluded from the ensemble average. Such selective elimination of the narrowest modes should have led to an overestimation of $\delta\nu$. The absence of deviation from equation (25) indicates that amplification

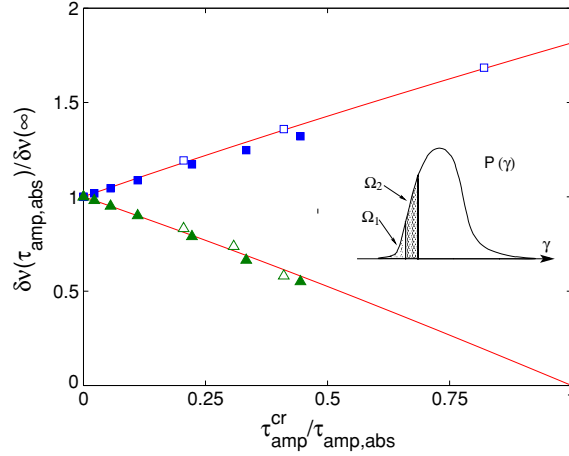


Figure 11. Spectral correlation width $\delta\nu$ as a function of amplification time τ_{amp} (triangles) or absorption time τ_{abs} (squares). $\delta\nu$ is normalized to the value of the passive system ($\tau_{\text{amp/abs}} = \infty$), $\tau_{\text{amp/abs}}$ to $\tau_{\text{amp}}^{\text{cr}}$. Solid symbols correspond to $g_0 = 4.4$, open symbols to $g_0 = 9$. The solid curves are given by the diffusion theory. The inset is a schematic plot of $P(\gamma)$.

not only reduces the width of all non-lasing modes, but also enhances the weight of the quasimodes with narrower-than-average width (within Ω_2) in the averaging.

In figure 11, the diminishing correlation width $\delta\nu$ in the amplifying system signifies that the optical gain approaches the lasing threshold for the quasimode with average decay rate $\langle\gamma\rangle$. According to equation (25), $\delta\nu = 0$ when $\sin(L'/l_{\text{amp}})$ turns to zero at $L'/l_{\text{amp}} = \pi$. This ‘average’ lasing threshold agrees with the diffusive lasing threshold derived by Letokhov (1968). Our calculation shows that the (conditional) average mode linewidth $\delta\nu$ can become smaller than the average mode spacing $d\nu$ before the diffusive lasing threshold is reached. Namely, with increasing gain, $\delta\nu$ decreases to $d\nu$ before reaching zero. This means that the effective Thouless number $\delta = \delta\nu/d\nu$ can be reduced to below 1 by coherent amplification for a system that is diffusive in the absence of gain.

Figure 12 shows the nonlocal part of spatial intensity correlation function, $C(\Delta r) - C_1(\Delta r)$, as a function of $\tau_{\text{amp}}^{\text{cr}}/\tau_{\text{amp}}$ in samples of $g_0 = 4.4$ and 9.0 . $\tau_{\text{amp}}^{\text{cr}} = L'/\pi v_e$ is the critical amplification time for lasing in the quasimode with average decay rate. According to Sebbah *et al* (2002) and Pnini (2001), spatial variation and absorption contribution should factorize. Accounting for terms up to $1/g_0^2$, we obtain the ‘negative absorption’ expression for nonlocal intensity correlation (Garcia *et al* 1993, Pnini and Shapiro 1991, Kogan and Kaveh 1992, van Rossum and Nieuvenhuizen 1993, Sebbah *et al* 2002, Brouwer 1998):

$$C(\Delta r, s = L/l_{\text{amp}}) - |C_E(\Delta r, s)|^2 = (1 + F(\Delta r)) \times \left[\frac{1}{4gs} \frac{2s(2 - \cos 2s) - \sin 2s}{\sin^2 s} + \frac{4}{g^2} \frac{\sin^2 s}{s^2} \times \left(\frac{2s^2 - s \cot s + 1}{16 \sin^2 s} - 3 \frac{s^2 + s \cot s + 1}{16 \sin^4 s} + \frac{3s^2}{8 \sin^6 s} \right) \right], \quad (26)$$

where $F(\Delta r) = |C_E(\Delta r)|^2$. The inset of figure 12 shows the profile of $C(\Delta r) - C_1(\Delta r)$, normalized to its value at $\Delta r = 0$. For passive, absorbing and amplifying systems, the spatial variation of $C - C_1$ with Δr is almost the same. In particular, the value of $C - C_1$ at $\Delta r \rightarrow \infty$ is exactly half of that at $\Delta r = 0$, in agreement with $[1 + F(\Delta r)]$ dependence.

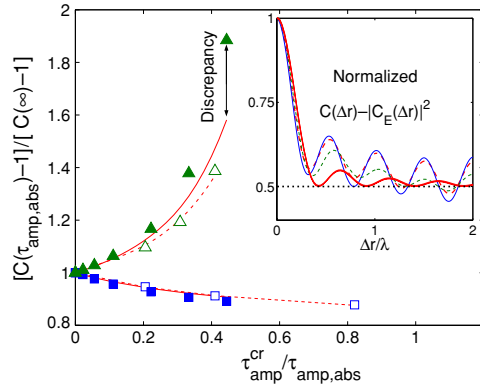


Figure 12. $C - C_1$ at $\Delta r = 0$ and $\Delta \nu = 0$ in absorbing (squares) and amplifying (triangles) systems. Solid symbols correspond to $g_o = 4.4$, open symbols to $g_o = 9$. Solid and dashed curves are obtained from equation (26) without any fitting parameters. The inset compares the dependence of $C - C_1$ on Δr with $[F(\Delta r) + 1]/2$ (thick line). Thin solid, dotted and dashed lines represent passive, absorbing and amplifying systems as in figure 10.

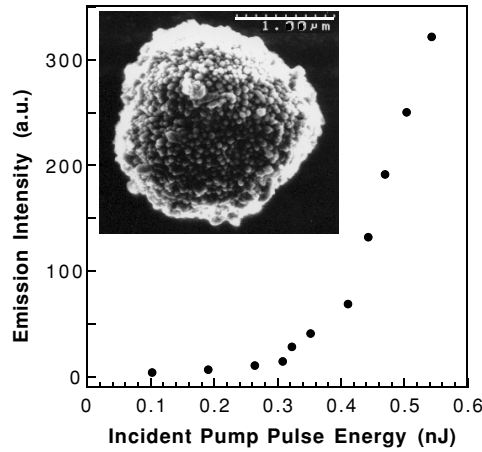


Figure 13. Frequency dependence of nonlocal contribution to $C(\Delta \nu)$ normalized to its value at $\Delta \nu = 0$. The inset shows the local contribution $C_1(\Delta \nu) = |C_E(\Delta \nu)|^2$. System parameters and symbol notation are the same as in figure 10. The open (solid) arrow shows the direction of increasing gain (absorption).

This suggests that amplification increases the nonlocal correlations at every Δr uniformly. Therefore, the enhancement can be characterized by a single number, e.g., the value of $C - C_1$ at $\Delta r = 0$ as shown in figure 12. In two absorbing samples of $g_o = 4.4$ and 9, the decrease of nonlocal correlations is in good agreement with the diffusion prediction. For amplifying media, only when the fraction of omitted lasing realizations is small, equation (26) adequately describes the nonlocal correlations of the transmitted intensity. For high gain, we see strong deviations: even after removing the lasing realizations, nonlocal correlation still exceeds the ‘negative absorption’ prediction (equation (26)). The deviation becomes more pronounced as g_o decreases. The rapid increase of nonlocal correlation with gain is caused by enhanced contribution from long trajectories that cross upon themselves.

Finally, we calculate the spectral correlations of transmitted intensities. Figure 13 reveals the changes of $C_1(\Delta \nu)$ and $C(\Delta \nu) - C_1(\Delta \nu)$ caused by amplification or absorption. The

frequency separation $\Delta\nu$ is normalized to the average mode linewidth $\delta\nu$ of the passive system. $C(\Delta\nu) - C_1(\Delta\nu)$ is also normalized to its value at $\Delta\nu = 0$. Both C_1 and $C - C_1$ are narrowed by amplification and broadened by absorption. While the narrowing of $C_1(\Delta\nu)$ with increasing gain is similar to that of a passive system with decreasing g_o , the narrowing of $C(\Delta\nu) - C_1(\Delta\nu)$ is just the opposite. When a passive system approaches the localization transition, the most conducting channels dominate the transport and correlations. Thus, after normalizing $\Delta\nu$ by the correlation width $\delta\nu$, $C(\Delta\nu) - C_1(\Delta\nu)$ is widened as g_o decreases in a passive system, but it is narrowed with the fixed g_o and increasing gain. This remarkable difference illustrates that in a passive system near the localization transition, the quasimodes with larger-than-average width dominate the transport, while in a diffusive system with sufficient gain, the quasimodes with narrower-than-average width are preferably amplified and become dominant.

6.2. Statistical distribution of transmission coefficient in amplifying random medium

Our FDTD algorithm can also be applied to the numerical study on fluctuations of transmission and reflection (Yamilov and Cao 2004b). From the numerical data, we extract the statistical distributions of the following quantities: (i) T_{ab} (R_{ab}), the transmission (reflection) coefficient from an incoming channel a to an outgoing channel b ; (ii) $T_a = \sum_b T_{ab}$ ($R_a = \sum_b R_{ab}$), total transmission (reflection) coefficient from channel a to all outgoing channels; (iii) $g_T = \sum_{a,b} T_{ab}$ ($g_R = \sum_{a,b} R_{ab}$), transmittance (reflectance). The dimensionless conductance $g_c \equiv \langle g_T \rangle$. Our numerical calculation reveals the quantitative changes brought by amplification to these distributions. In the following, the numerical result of statistical distribution of normalized transmission coefficient $s_{ab} = T_{ab}/\langle T_{ab} \rangle$ is presented as an example.

We again consider the quasi-1D system described in the last subsection. $P(s_{ab})$ is obtained by collecting the data of transmitted intensity from many random configurations. Among them, there exist rare configurations that could lase even in the presence of low gain. Light intensity would diverge if gain depletion were neglected. In the diffusion regime $g_o \gg 1$, this problem is limited only to the immediate vicinity of the diffusive lasing threshold (Zyuzin 1995). For the systems we consider, $g_o < 10$, strong fluctuation of the lasing threshold results in a non-negligible percentage of lasing realizations even at moderate gain (i.e., not very close to the diffusive lasing threshold). Although gain saturation could prevent the divergence of light intensity, the actual value of the saturated intensity depends on the properties of the gain material. In order to eliminate any material-dependent effect on $P(s_{ab})$, we disregard the contributions of the lasing configurations to the intensity distribution. To compare the effect of amplification to that of absorption, we also calculate $P(s_{ab})$ in the same random system with absorption.

Figure 14 compares $P(s_{ab})$ in a quasi-1D sample ($g_o = 2.2$) with gain or absorption to that without it. $\tau_{\text{amp}} = -\tau_{\text{abs}} = 5\tau_{\text{amp}}^{\text{cr}}$. Even at such low level of gain, some of the random realizations lase, due to strong fluctuation of lasing threshold. The numerical results presented in figure 14 contain only the contributions from non-lasing realizations. Figure 14 shows that the presence of gain leads to an increase of $P(s_{ab})$ in the regions $s_{ab} \ll 1$ and $s_{ab} \gg 1$, and therefore an enhancement of intensity fluctuations. The effect of absorption is exactly the opposite.

$P(s_{ab})$ in an amplifying system can be well fitted with the following distribution:

$$P(s_{ab}) = \int_0^\infty \frac{ds_a}{s_a} P(s_a) e^{-s_{ab}/s_a}, \quad (27)$$

where the distribution of the normalized total transmission coefficient $s_a = T_a/\langle T_a \rangle$ is

$$P(s_a) = \int_{-i\infty}^{i\infty} \frac{dx}{2\pi i} e^{[xs_a - \Phi_0(g',x)]}, \quad (28)$$

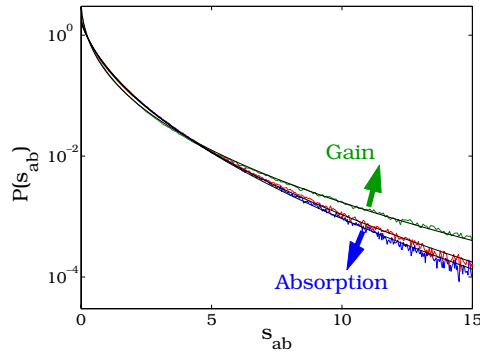


Figure 14. Numerically calculated $P(s_{ab})$ for a sample of $g_o = 2.2$ with and without gain/absorption. The arrows mark the directions of increasing gain and absorption. Dashed lines represent the fit with equations (27) and (28); $g' = 1.5$ (absorption), 1.25 (passive) and 0.65 (gain).

with $\Phi_0(g', x) = g' \ln^2(\sqrt{1 + x/g'} + \sqrt{x/g'})$. Equation (28) is derived originally by Kogan *et al* under the assumption of $g_c \gg 1$, thus $g' = g_c = g_o$ (Kogan *et al* 1993). Genack and co-workers demonstrate that equation (28) works well even for moderate values of $g_c \sim 10$ and in the presence of significant absorption (Stoytchev and Genack 1997, 1999, Chabanov *et al* 2000, Genack and Chabanov 2001). Based on the statistics of s_{ab} , the localization criterion,

$$g' \equiv \frac{2}{3} \text{var}(s_a) \equiv \frac{4}{3} [\text{var}(s_{ab}) - 1], \quad (29)$$

equal to unity is surmised, that is applicable to absorbing system (Chabanov *et al* 2000). The above definition of g' can be used, irrespective of whether equation (28) holds. However, if equation (28) is applicable, g' obtained from equation (29) should match the one obtained from the fit of the entire distribution of s_{ab} with equations (27) and (28) (Kogan and Kaveh 1995). Our numerical results demonstrate that equations (27) and (28) still hold in an amplifying system. However, amplification reduces the value of g' , while absorption increases it.

Figure 15 shows the effect of amplification or absorption on g' for three samples of $g_o = 7.6, 4.4, 2.2$. δ is obtained from the calculation of $C_E(\Delta\nu)$. The superlinear increase of $1/g'$ with $1/\delta$ in figure 15 illustrates that g' decreases significantly faster than δ with increasing gain. This indicates that intensity fluctuations are more sensitive to amplification than the average mode linewidth $\delta\nu$. In contrast, the absorption causes a reduction of fluctuations. The sublinear decrease of $1/g'$ with $1/\delta$ in figure 15 reveals that g' increases slower than δ with increasing absorption. The dependence of g' on the absorption time τ_{abs} can be determined perturbatively from the known result for $\text{var}(s_{ab})$ in an absorbing system of $g_o \gg 1$:

$$\frac{4}{3g'_o(g_o, \tau_{abs})} \equiv \text{var}(s_{ab}) - 1 = \frac{4}{3g_o} A_2(\tau_{abs}) + \frac{8}{15g_o^2} A_3(\tau_{abs}), \quad (30)$$

where $A_2(\tau_{abs})$ and $A_3(\tau_{abs})$ are given in Sebbah *et al* (2002) and Pnini (2001). The expressions for A_i are derived for absorbing systems, where τ is positive. In the case of amplifying media, τ_{amp} is negative, the contribution of lasing realizations should be omitted to avoid the divergence of $\text{var}(s_{ab})$. For the two samples of larger g_o , we compare our data to equation (30) in the inset of figure 15. $\delta(g_o, \tau_{amp})$ is found from the width of $|C_E(\Delta\nu)|^2$. By eliminating τ_{amp} from $g'(g_o, \tau_{amp})$ and $\delta(g_o, \tau_{amp})$, we obtain $g'(\delta)$, shown as the solid lines in figure 15. The

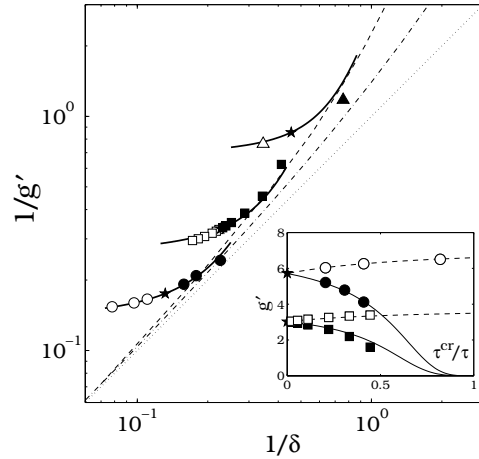


Figure 15. Numerical data of $1/g'$ versus $1/g_0$ for samples of $g_0 = 7.6$ (circles), 4.4 (squares), 2.2 (triangles). In the zeroth order of $1/g_0$, $g'(g_0) = g_0$ (dotted line). The dash-dotted line is $g'(g_0)$ with the first-order correction. Dashed line plots the exact solution $g(g_0)$ from Mirlin (2000). The inset shows the linear dependence of δ on g_0 . The solid line has a slope of 1.

deviations of our data points from the solid line increase with a decrease in g_0 , because the contributions of the higher order terms in $1/g_0$ cannot be neglected.

Amplification results in an increase of g' and δ , but a decrease of g_c . The changes caused by absorption are the opposite for g' and δ , but the same for g_c . With the increase of absorption, δ increases without a bound, while $g'(\tau_{\text{abs}} \rightarrow 0)$ approaches $(4/3)g'(\tau_{\text{abs}} \rightarrow \infty)$ in the limit $g_c \gg 1$. In sharp contrast, in amplifying systems g' diminishes superlinearly with $\tau_{\text{amp}}^{\text{cr}}/\tau_{\text{amp}}$ (inset of figure 15), while δ decreases almost linearly with $\tau_{\text{amp}}^{\text{cr}}/\tau_{\text{amp}}$ as shown in figure 11. Our numerical result in the inset of figure 15 also suggests that g' fall below unity prior to δ in an amplifying system. Therefore, g' is more sensitive to amplification but less sensitive to absorption than δ .

7. Closing remark

Over the last few years, random lasers with coherent feedback have been realized in many material systems such as semiconductor nanostructures (Cao *et al* 1998, Mitra and Thareja 1999, Thareja and Mitra 2000, Sun *et al* 2003, Yu *et al* 2004a, 2004b, Leong *et al* 2004, Hsu *et al* 2005, Yuen *et al* 2005a, Lau *et al* 2005), organic films and nanofibres (Anni *et al* 2003, Guochi *et al* 2004, Klein *et al* 2005) and hybrid organic–inorganic composites (Yokoyama and Mashiko 2003, Anglos *et al* 2004, Song *et al* 2005). Various schemes have been proposed to improve the performance of random lasers, e.g., application of external feedback to reduce the lasing threshold and control the output direction of laser emission (Cao *et al* 1999a), optimal tuning of random lasing modes through collective particle resonance (Ripoll *et al* 2004), coupled-cavity ZnO thin-film random laser for high-power one-mode operation (Yu and Leong 2004), one-mirror random laser for quasi-continuous operation (Feng and Ueda 2003, Feng *et al* 2004) and waveguide random laser for directional output (Yuen *et al* 2005b, Watanabe *et al* 2005). The progress is so rapid that it is impossible to detail all of the advances. Next, I briefly mention a few of them.

7.1. Partially ordered random laser

One way of reducing the random laser threshold is to incorporate some degree of order into an active random medium (Chang *et al* 2003, Yamilov and Cao 2004a, Burin *et al* 2004). Shkunov *et al* have observed both photonic lasing and random lasing in dye-infiltrated opals (Shkunov *et al* 2001). However, random lasing has higher threshold than photonic lasing. We numerically simulate lasing in a random system with variable degree of order. When disorder is introduced to a perfectly ordered system, the lasing threshold is reduced. At a certain degree of disorder, the lasing threshold reaches a minimum. Then, it starts rising with further increase of disorder. Therefore, there exists an optimum degree of order for minimum lasing threshold. We map out the transition from full order to complete disorder and identify five scaling regimes for the mean lasing threshold versus the system size L . For increasing degree of disorder, the five regimes are (a) photonic band-edge, $1/L^3$, (b) transitional super-exponential, (c) bandgap-related exponential, (d) diffusive, $1/L^2$, and (e) disorder-induced exponential. Experimentally, we have fabricated disordered photonic crystal lasers (Wu *et al* 2004a). The most efficient lasing modes are localized defect states near the edge of a photonic bandgap. Such defect states are formed by structural disorder in a 2D triangle lattice. Another advantage of the partially ordered random laser is efficient pumping. For example, in a 1D random stack of resonant dielectric layers, the pump wavelength can be tuned to a pass band while the emission wavelength stays in a stop band (Feng and Ueda 2004). Then, the pump light penetrates into the sample, while the emission is confined inside the system. As a result, the lasing threshold can be significantly reduced.

7.2. Mode interaction

The interaction of lasing modes in a random medium is interesting but complicated. Gain competition may lead to mode repulsion in real space for homogeneously broadened gain spectrum or in frequency domain for inhomogeneously broadened gain spectrum (Cao *et al* 2003a, Jiang *et al* 2004). In addition, the inhomogeneity of dielectric constant $\epsilon(\mathbf{r})$ modifies the ortho-normalization condition for the quasimodes and introduces a linear coupling between the quasimodes mediated by the polarization of the gain medium (Deych 2005). Finally, the overlapping quasimodes may couple via external bath, that generates excess noise and broadens the lasing linewidth (Patra *et al* 2000, Frahm *et al* 2000, Schomerus *et al* 2000).

7.3. Nonlinear random laser

Random laser offers an opportunity to study the interplay between nonlinearity and localization. Nonlinear effect is strong in a random laser because the nonlinear coefficient is resonantly enhanced at the lasing frequency and the light intensity is high due to spatial confinement in random media. Noginov *et al* demonstrate second-harmonic generation in a mixture of powders of laser and frequency doubling materials (Noginov *et al* 1998). Our recent study on the dynamic nonlinear effect in a random laser illustrates that the third-order nonlinearity not only changes the frequency and size of the lasing modes, but also modifies the laser emission intensity and laser pulse width (Liu *et al* 2003). How nonlinearity affects random lasing process depends on how fast the nonlinear response is. We find two regimes depending on the relative values of two time scales, one is the nonlinear response time, the other is the lifetime of the lasing state. For slow nonlinear response, collective scattering of many particles determines the build-up of a lasing mode. Nonlinearity changes the lasing output through modification of spatial size of the lasing mode. However, when the nonlinear

response is faster than the build-up of a lasing mode, the lasing mode cannot respond fast enough to the nonlinear refractive index change. Rapid change of the phase of scattered waves undermines the interference effect of multiple scattering. Instead, the nonlinear effect of single particle scattering becomes dominant. Strong nonlinearity could lead to temporal instability. One application of optical nonlinearity is upconversion lasing in random media via two-photon or multi-photon pumping (Zacharakis *et al* 2002, Fujiwara and Sasaki 2004). Small two-photon/multi-photon absorption coefficient and weak scattering at long pumping wavelength allow deep penetration of the pump light into a 3D random medium, thus improving the spatial confinement of laser emission (Burin *et al* 2003b).

The potential applications of random lasers will not be discussed here; the reader is referred to, e.g., Lawandy (1994), Wiersma (2000), Rand (2003) and Cao (2005). The latest theoretical and experimental studies provide insight into the physical mechanisms for lasing in random media (Patra 2003a, Florescu and John 2004c, Kretschmann and Maradudin 2004, Noginov *et al* 2004a, 2004b, 2004c, Polson and Vardeny 2004, Mujumdar *et al* 2004a, Gottardo *et al* 2004, Li *et al* 2005, Lubatsch *et al* 2005, Vasa *et al* 2005). However, our understanding of random lasers is far from complete. New ideas and surprises arise frequently, maintaining the momentum of random laser study. For example, Rand and co-workers investigate the electrical generation of stationary light (evanescent wave) in ultrafine laser crystal powder (Redmond *et al* 2004). Dice *et al* report the surface-plasmon-enhanced random laser emission from a suspension of silver nanoparticles in a laser dye (Dice *et al* 2005). Mujumdar *et al* observe emission spikes even when the transport mean free path is much longer than the pump spot diameter (Mujumdar *et al* 2004b). The emission spikes are attributed to amplification of spontaneous emission along very long trajectories, because they are distinct from shot to shot and thus intrinsically stochastic. However, Polson and Vardeny use the powerful PFT technique to reveal the underlying periodicity of the emission peaks in similar random samples (Polson and Vardeny 2005). The ensemble-averaged power Fourier transform of random laser emission spectra contains a sharp, well-resolved Fourier component and its harmonics, which are characteristic of a well-defined laser resonator. The formation of such resonators remain to be understood. Nevertheless, puzzles like these make the random laser an exciting field to explore!

Acknowledgments

I wish to thank my co-workers on the study of random lasers. J Y Xu, Y Ling, X Wu, Y G Zhao and Professor Prem Kumar contributed to the experimental work on random lasers. Drs A Yamilov, A L Burin, B Liu, S-H Chang, Professors S T Ho, A Taflove, M A Ratner and G C Schatz conducted theoretical studies of random lasers. Professor R P H Chang and his students E W Seelig and X Liu fabricated ZnO nanorods and nanoparticles. We enjoyed a fruitful collaboration with Professor C M Soukoulis and Dr Xunya Jiang on the simulation of random laser. Stimulated discussions are acknowledged with Drs A A Asatryan, A A Chabanov, Ch M Brikina, L Deych, M Giudici, B Grémaud, F Haake, G Hackenbroich, A Z Genack, S John, R Kaiser, T Kottos, V M Letokhov, C Miniatura, M A Noginov, M Patra, M E Raikh, S C Rand, P Sebbah, B Shapiro, C M de Sterke, J Tredicce, C Vanneste, Z V Vardeny, C Viviescas, T Wellens and D S Wiersma. Our research programme is partly sponsored by the National Science Foundation through the grants ECS-9877113, DMR-0093949 and ECS-0244457, and by the David and Lucille Packard Foundation, the Alfred P Sloan Foundation and the Northwestern University Materials Research Center.

References

- Altshuler B L, Kravtsov V E and Lerner I V 1991 *Mesoscopic Phenomena in Solids* ed B L Altshuler, P A Lee and R A Webb (Amsterdam: North-Holland)
- Ambartsumyan R V, Basov N G and Letokhov V S 1968 *Sov. Phys.—JETP* **26** 1109
- Ambartsumyan R V, Bazhulin S P, Basov N G and Letokhov V S 1970 *Sov. Phys.—JETP* **31** 234
- Ambartsumyan R V, Kryukov P G, Letokhov V S and Matveets Yu A 1967 *JETP Lett.* **5** 378
- Anglos D, Stassinopoulos A, Das R N, Zacharakis G, Psyllaki M, Jakubiak R, Vaia R A, Giannelis E P and Anastasiadis S H 2004 *J. Opt. Soc. Am. B* **21** 208
- Anni M, Lattante S, Cingolani R, Gigli G, Barbarella G and Favaretto L 2003 *Appl. Phys. Lett.* **83** 2754
- Anni M, Lattante S, Stomeo T, Cingolani R, Gigli G, Barbarella G and Favaretto L 2004 *Phys. Rev. B* **70** 195216
- Apalkov V M and Raikh M E 2005 *Phys. Rev. B* **71** 054203
- Apalkov V M, Raikh M E and Shapiro B 2002 *Phys. Rev. Lett.* **89** 016802
- Apalkov V M, Raikh M E and Shapiro B 2003 *The Anderson Transition and its Ramifications—Localization, Quantum Interference, and Interactions (Lecture Notes in Physics vol 630)* ed T Brandes and S Kettermann (Berlin: Springer) p 119
- Apalkov V M, Raikh M E and Shapiro B 2004a *J. Opt. Soc. Am. B* **21** 132
- Apalkov V M, Raikh M E and Shapiro B 2004b *Phys. Rev. Lett.* **92** 066601
- Beenakker C W J 1996 *Phys. Rev. Lett.* **76** 1368
- Beenakker C W J 1998 *Phys. Rev. Lett.* **81** 1829
- Beenakker C W J 1999 *Diffusive Waves in Complex Media (NATO Advanced Studies Institute, Series C: Mathematical and Physical Sciences vol 531)* ed J-P Fouquet (Dordrecht: Kluwer) pp 137–64
- Berkovits R and Feng S 1994 *Phys. Rep.* **238** 136
- Brouwer P Q 1998 *Phys. Rev. B* **57** 10526
- Burin A L, Cao H and Ratner M A 2003a *Physica B* **338** 212
- Burin A L, Cao H and Ratner M A 2003b *IEEE J. Select. Top. Quantum Electron.* **9** 124
- Burin A L, Cao H, Schatz G C and Ratner M A 2004 *J. Opt. Soc. Am. B* **21** 121
- Burin A L, Ratner M A, Cao H and Chang R P H 2001 *Phys. Rev. Lett.* **87** 215503
- Burin A L, Ratner M A, Cao H and Chang S-H 2002 *Phys. Rev. Lett.* **88** 093904
- Burkov A A and Zyuzin A Yu 1996 *JETP Lett.* **63** 878
- Burkov A A and Zyuzin A Yu 1997 *Phys. Rev. B* **55** 5736
- Cao H 2003 *Waves Random Media* **13** R1
- Cao H 2005 *Opt. Photon. News* **16** 24
- Cao H, Jiang X, Ling Y, Xu J Y and Soukoulis C M 2003a *Phys. Rev. B* **67** 161101
- Cao H, Ling Y, Xu J Y and Burin A L 2002 *Phys. Rev. E* **66** 25601
- Cao H, Ling Y, Xu J Y, Cao C Q and Kumar P 2001 *Phys. Rev. Lett.* **86** 4524
- Cao H, Xu J Y, Chang S-H and Ho S T 2000a *Phys. Rev. E* **61** 1985
- Cao H, Xu J Y, Chang S-H, Ho S T, Seelig E W, Liu X and Chang R P H 2000b *Phys. Rev. Lett.* **84** 5584
- Cao H, Xu J Y, Ling Y, Burin A L, Seelig E W, Liu X and Chang R P H 2003b *IEEE J. Select. Top. Quantum Electron.* **9** 111
- Cao H, Xu J Y, Seelig E W and Chang R P H 2000c *Appl. Phys. Lett.* **76** 2997
- Cao H, Zhao Y G, Liu X, Seelig E W and Chang R P H 1999a *Appl. Phys. Lett.* **75** 1213
- Cao H, Zhao Y G, Ong H C, Ho S T, Dai J Y, Wu J Y and Chang R P H 1998 *Appl. Phys. Lett.* **73** 3656
- Cao H, Zhao Y G, Ong H C, Ho S T, Seelig E Q, Wang Q H and Chang R P H 1999b *Phys. Rev. Lett.* **82** 2278
- Chabanov A A, Stoytchev M and Genack A Z 2000 *Nature* **404** 850
- Chabanov A A, Zhang Z Q and Genack A Z 2003 *Phys. Rev. Lett.* **90** 203903
- Chang S-H, Cao H and Ho S T 2003 *IEEE J. Quantum Electron.* **39** 364
- Chang S-H, Taflove A, Yamilov A, Burin A L and Cao H 2004 *Opt. Lett.* **29** 917
- Deng W, Wiersma D and Zhang Z Q 1997 *Phys. Rev. B* **56** 178
- Deych L I 2005 *Phys. Rev. Lett.* **95** 043902
- de Oliveira P C, Perkins A E and Lawandy N M 1996 *Opt. Lett.* **21** 1685
- Dice G D, Mujumdar S and Elezzabi A Y 2005 *Appl. Phys. Lett.* **86** 131105
- Falko V I and Efetov K B 1995a *Europhys. Lett.* **32** 627
- Falko V I and Efetov K B 1995b *Phys. Rev. B* **52** 17413
- Feng Y, Bisson J-F, Lu J, Huang S, Takaichi K, Shirakawa A, Musha M and Ueda K 2004 *Appl. Phys. Lett.* **84** 1040
- Feng Y and Ueda K 2003 *Phys. Rev. A* **68** 025803
- Feng Y and Ueda K 2004 *Opt. Express* **12** 3307
- Florescu L and John S 2004a *Phys. Rev. Lett.* **93** 013602

- Florescu L and John S 2004b *Phys. Rev. E* **69** 046603
- Florescu L and John S 2004c *Phys. Rev. E* **70** 036607
- Frahm K M, Schomerus H, Patra M and Beenakker C W J 2000 *Europhys. Lett.* **49** 48
- Freilikher V, Pustilnik M and Yurkevich I 1997 *Phys. Rev. B* **56** 5974
- Freund I and Eliyahu D 1992 *Phys. Rev. A* **45** 6133
- Frolov S V, Vardeny Z V, Yoshino K, Zakhidov A and Baughman R H 1999a *Phys. Rev. B* **59** R5284
- Frolov S V, Vardeny Z V, Yoshino K, Zakhidov A and Baughman R H 1999b *Opt. Commun.* **162** 241
- Fujiwara H and Sasaki K 2004 *Japan. J. Appl. Phys. L* **43** 1337
- Fyodorov Y V and Mirlin A 1994 *Int. J. Mod. Phys. B* **8** 3795
- Fyodorov Y V and Mirlin A 1995 *Phys. Rev. B* **51** 13403
- Garcia N, Genack A Z, Pnini R and Shapiro B 1993 *Phys. Lett. A* **176** 458
- Genack A Z and Chabanov A A 2001 *Waves and Imaging Through Complex Media* ed P Sebbah (Dordrecht: Kluwer)
- Gottardo S, Cavalieri S, Yaroshchuk O and Wiersma D S 2004 *Phys. Rev. Lett.* **93** 263901
- Hackenbroich G, Viviescas C and Haake F 2002 *Phys. Rev. Lett.* **89** 083902
- Hackenbroich G, Viviescas C and Haake F 2003 *Phys. Rev. A* **68** 063805
- Herrmann J and Wilhelm B 1998 *Appl. Phys. B* **66** 305
- Hsu H-C, Wu C-Y and Hsieh W-F 2005 *J. Appl. Phys.* **97** 064315
- Jiang X, Li Q and Soukoulis C M 1999 *Phys. Rev. B* **59** 9007
- Jiang X, Song F, Soukoulis C M, Zi J, Joannopoulos J D and Cao H 2004 *Phys. Rev. B* **9** 104202
- Jiang X and Soukoulis C M 1999 *Phys. Rev. B* **59** 6159
- Jiang X and Soukoulis C M 2000 *Phys. Rev. Lett.* **85** 70
- Jiang X and Soukoulis C M 2002 *Phys. Rev. E* **65** 025601
- John S 1991 *Phys. Today* **44** 32
- John S and Pang G 1996 *Phys. Rev. A* **54** 3642
- Joshi S K and Jayannavar 1997 *Phys. Rev. B* **56** 12038
- Klein S, Crégut O, Gindre D, Boeglin A and Dorkenoo K D 2005 *Opt. Express* **13** 5387
- Kogan E and Kaveh M 1992 *Phys. Rev. B* **45** 1049
- Kogan E and Kaveh M 1995 *Phys. Rev. B* **52** 3813
- Kogan E, Kaveh M, Baumgartner R and Berkovits R 1993 *Phys. Rev. B* **48** 9404
- Kottos T, Ossipov A and Geisel T 1995 *Phys. Rev. B* **52** 3813
- Kottos T, Ossipov A and Geisel T 2003 *Phys. Rev. E* **68** 066215
- Kretschmann M and Maradudin A A 2004 *J. Opt. Soc. Am. B* **21** 150
- Kumar N 2001 *Physica E* **9** 356
- Lau S P, Yang H Y, Yu S F, Li H D, Tanemura M, Okita T, Hatano H and Hng H H 2005 *Appl. Phys. Lett.* **87** 013104
- Lawandy N M 1994 *Photon. Spectra* **28** 119
- Leong E, Chong M K, Yu S F and Pita K 2004 *IEEE Photon. Technol. Lett.* **16** 2418
- Letokhov V S 1968 *Sov. Phys.—JETP* **26** 1246
- Li Q, Ho K M and Soukoulis C M 2001 *Physica B* **296** 78
- Li S, Wang Z-J, Chen L-S, Sun X and George T F 2005 *Appl. Phys. Lett.* **86** 171109
- Ling Y, Cao H, Burin A L, Ratner M A, Liu X and Chang R P H 2001 *Phys. Rev. A* **64** 063808
- Liu B, Yamilov A, Ling Y, Xu J Y and Cao H 2003 *Phys. Rev. Lett.* **91** 063903
- Lubatsch A, Kroha J and Busch K 2005 *Phys. Rev. B* **71** 184201
- Markushev V M, Ryzhkov V M, Briskina Ch M, Cao H, Zadorozhnyayac L A, Li L E, Gevargizov E I and Demianets L N 2005 *Laser Phys.* at press
- Milner V and Genack A Z 2005 *Phys. Rev. Lett.* **94** 073901
- Mirlin A D 2000 *Phys. Rep.* **326** 260
- Mishchenko E G, Patra M and Beenakker C W J 2001 *Eur. Phys. J. D* **13** 289
- Misirpashaev T Sh and Beenakker C W J 1998 *Phys. Rev. A* **57** 2041
- Mitra A and Thareja R K 1999 *Mod. Phys. Lett. B* **23** 1075
- Mujumdar S, Cavalieri S and Wiersma D S 2004a *J. Opt. Soc. Am.* **21** 201
- Mujumdar S, Ricci M, Torre R and Wiersma D S 2004b *Phys. Rev. Lett.* **93** 053903
- Nikolić B 2001 *Phys. Rev. B* **64** 014203
- Noginov M A, Egarievwe S U, Noginova N E, Wang J C and Caulfield H J 1998 *J. Opt. Soc. Am. B* **15** 2854
- Noginov M A, Novak J and Williams S 2004a *Phys. Rev. A* **70** 043811
- Noginov M A, Novak J and Williams S 2004b *Phys. Rev. A* **70** 063810
- Noginov M A, Zhu G, Fowlkes I and Bahoura M 2004c *Laser Phys. Lett.* **1** 291
- Ossipov A, Kottos T and Geisel T 2002 *Phys. Rev. E* **65** 055209

- Ossipov A, Kottos T and Geisel T 2003 *Europhys. Lett.* **62** 719
- Paasschens J C J, Misirpashaev T Sh and Beenakker C W J 1996 *Phys. Rev. B* **54** 11887
- Patra M 2002 *Phys. Rev. A* **65** 043809
- Patra M 2003a *Phys. Rev. E* **67** 016603
- Patra M 2003b *Phys. Rev. E* **67** 065603
- Patra M and Beenakker C W J 1999 *Phys. Rev. A* **60** 4059
- Patra M, Schomerus H and Beenakker C W J 2000 *Phys. Rev. A* **61** 023810
- Peřinová V, Lukš A and Křepelka 2004 *J. Opt. B: Quantum Semiclass. Opt.* **6** S104
- Pnini R 2001 *Waves and Imaging Through Complex Media* ed P Sebbah (Dordrecht: Kluwer)
- Pnini R and Shapiro B 1991 *Phys. Lett. A* **157** 265
- Polson R C, Chipouline A and Vardeny Z V 2001a *Adv. Mater.* **13** 760
- Polson R C, Huang J D and Vardeny Z V 2001b *Synth. Met.* **119** 7
- Polson R C, Raikh M E and Vardeny Z V 2002 *C. R. Acad. Sci. Ser. IV (Phys. Astrophys.)* **3** 509
- Polson R and Vardeny Z V 2004 *Appl. Phys. Lett.* **85** 1289
- Polson R and Vardeny Z V 2005 *Phys. Rev. B* **71** 045205
- Pradhan P and Kumar N 1994 *Phys. Rev. B* **50** 9644
- Quochi F, Andreev A, Cordella F, Orrù R, Mura A, Bongiovanni G, Hoppe H, Sitter H and Sariciftci N S 2005 *J. Luminescence* **112** 321
- Quochi F, Cordella F, Orrù R, Communal J E, Verzeroli P, Mura A, Bongiovanni G, Andreev A, Sitter H and Sariciftci N S 2004 *Appl. Phys. Lett.* **84** 4454
- Ramakrishna S A, Das E K, Vijayagovindan G V and Kumar N 2000 *Phys. Rev. B* **62** 256
- Ramakrishna S A and Kumar N 2000 *Phys. Rev. B* **61** 3163
- Rand S 2003 *Opt. Photon. News* 33
- Redmond S M *et al* 2004 *J. Opt. Soc. Am. B* **21** 214
- Ripoll J, Soukoulis C M and Economou E N 2004 *J. Opt. Soc. Am. B* **21** 141
- Schomerus H, Frahm K M, Patra M and Beenakker C W J 2000 *Physica A* **278** 469
- Sebbah P, Hu B, Genack A Z, Pnini R and Shapiro B 2002 *Phys. Rev. Lett.* **88** 123901
- Sebbah P, Pnini R and Genack A Z 2000 *Phys. Rev. E* **62** 7348
- Sebbah P and Vanneste C 2002 *Phys. Rev. B* **66** 144202
- Seelig E W, Chang R P H, Yamilov A and Cao H 2003 *Mater. Chem. Phys.* **80** 257
- Shapiro B 1986 *Phys. Rev. Lett.* **57** 2168
- Shkunov M N, DeLong M C, Raikh M E, Vardeny Z V, Zakhidov A A and Baughman R H 2001 *Synth. Met.* **116** 485
- Siegman A 1986 *Lasers* (Mill Valley, CA: University Science Books)
- Song Q, Wang L, Xiao S, Zhou X, Liu L and Xu L 2005 *Phys. Rev. B* **72** 035424
- Soukoulis C M, Jiang X, Xu J Y and Cao H 2002 *Phys. Rev. B* **65** R041103
- Stassinopoulos A, Das R N, Giannelis E P, Anastasiadis S H and Anglos D 2005 *Appl. Surf. Sci.* **247** 18
- Stoytchev M and Genack A Z 1997 *Phys. Rev. Lett.* **79** 309
- Stoytchev M and Genack A Z 1999 *Opt. Lett.* **24** 262
- Sun B Q, Gal M, Gao Q, Tan H H, Jagadish C, Puzzer T, Ouyang L and Zou J 2003 *J. Appl. Phys.* **93** 5855
- Taflove A and Hagness S C 2000 *Computational Electrodynamics* (Boston, MA: Artech House)
- Taniguchi H, Tanosaki S, Tsujita K and Inaba H 1996 *IEEE J. Quantum Electron.* **32** 1864
- Thareja R K and Mitra A 2000 *Appl. Phys. B* **71** 181
- Tureci H E, Schwefel H G L, Jacquod Ph and Stone A D 2005 *Progress in Optics* ed E Wolf (Amsterdam: North-Holland)
- Tutov A V and Maradudin A A 1999 *Phys. Rev. B* **60** 12692
- Uski V, Mehlig B, Römer R A and Schreiber M 2001 *Phys. Rev. B* **63** 241101
- Uski V, Mehlig B and Schreiber M 2000 *Phys. Rev. B* **62** 7699
- Vanneste C and Sebbah P 2001 *Phys. Rev. Lett.* **87** 183903
- Vanneste C and Sebbah P 2005 *Phys. Rev. E* **71** 026612
- van Rossum M C W and Nieuvenhuizen Th M 1993 *Phys. Lett. A* **177** 452
- van Rossum M C W and Nieuvenhuizen Th M 1999 *Rev. Mod. Phys.* **71** 313
- Vasa P, Singh B P and Ayyub P 2005 *J. Phys. Condens. Matter* **17** 189
- Viviescas C and Hackenbroich G 2003 *Phys. Rev. A* **67** 013805
- Watanabe H, Oki Y, Maeda M and Omatsu T 2005 *Appl. Phys. Lett.* **86** 151123
- Weiss M, Mendez-Germudez J A and Kottos T 2005 *Preprint cond-matt/0509195*
- Wiersma D 2000 *Nature* **406** 132
- Wiersma D, van Albada M P and Lagendijk A 1995 *Phys. Rev. Lett.* **75** 1739
- Wu X, Yamilov A, Liu X, Li S, Dravid V P, Chang R P H and Cao H 2004a *Appl. Phys. Lett.* **85** 3657

- Wu X, Yamilov A, Noh H, Cao H, Seelig E W and Chang R P H 2004b *J. Opt. Soc. Am. B* **21** 159
- Yamilov A and Cao H 2004a *Phys. Rev. A* **69** 031803
- Yamilov A and Cao H 2004b *Phys. Rev. E* **70** 037603
- Yamilov A and Cao H 2005 *Phys. Rev. B* **71** 092201
- Yokoyama S and Mashiko S 2003 *Japan. J. Appl. Phys.* **42** L970
- Yoshino K, Tatsuhara S, Kawagishi Y and Ozaki M 1999 *Appl. Phys. Lett.* **74** 2590
- Yu S F and Leong E S P 2004 *IEEE J. Quantum Electron.* **40** 1186
- Yu S F, Yuen C, Lau S P and Lee H W 2004a *Appl. Phys. Lett.* **84** 3244
- Yu S F, Yuen C, Lau S P, Park W I and Yi G-C 2004b *Appl. Phys. Lett.* **84** 3241
- Yuen C, Yu S F, Leong E S P, Yang H Y and Hng H H 2005a *IEEE J. Quantum Electron.* **41** 970
- Yuen C, Yu S F, Leong E S P, Yang H Y, Lau S P, Chen N S and Hng H H 2005b *Appl. Phys. Lett.* **86** 031112
- Zacharakis G, Papadogiannis N A and Papazoglou T G 2002 *Appl. Phys. Lett.* **81** 2511
- Zhang Z Q 1995 *Phys. Rev. B* **52** 7960
- Zyuzin A Yu 1994 *Europhys. Lett.* **26** 517
- Zyuzin A Yu 1995 *Phys. Rev. E* **51** 5274

Erratum

Review on latest developments in random lasers with coherent feedback

H Cao 2005 *J. Phys. A: Math. Gen.* **38** 10497–10535

Figures 3 and 13 were inadvertently switched during the typesetting process. The figures are shown below with correct numbering and captions.

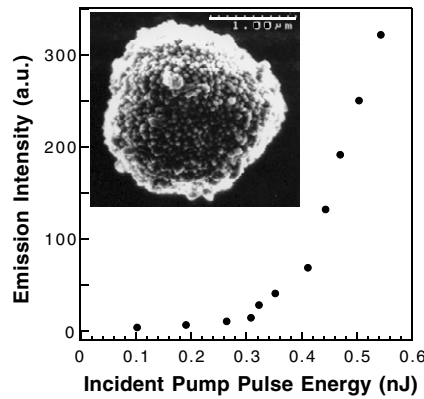


Figure 3. Spectrally integrated intensity of emission from the ZnO microcluster as a function of the incident pump pulse energy. The inset is the SEM image of the microcluster.

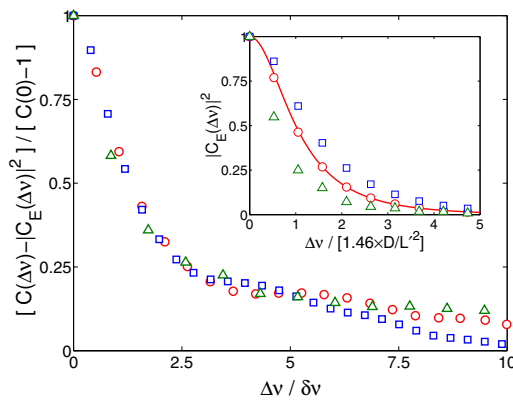


Figure 13. Frequency dependence of nonlocal contribution to $C(\Delta\nu)$ normalized to its value at $\Delta\nu = 0$. The inset shows the local contribution $C_1(\Delta\nu) = |C_E(\Delta\nu)|^2$. System parameters and symbol notations are the same as in Fig. 10. The open (solid) arrow shows the direction of increasing gain (absorption).